NASA CONTRACTOR REPORT

NASA CR-372

APPLICATION OF WEDGE DIFFRACTION TO ANTENNA THEORY

by R. C. Rudduck

Prepared under Contract No. NsG-448 *by*
OHIO STATE UNIVERSITY
Columbus, Ohio
for

NATIONAL AERONAUTICS AND SPACE ADMINISTRATION - WASHINGTON, D. C. - JANUARY 1966

NASA CR-372

APPLICATION OF WEDGE DIFFRACTION TO ANTENNA THEORY

By R. C. Rudduck

Prepared under Grant No. NsG-448 by
OHIO STATE UNIVERSITY
Columbus, Ohio

for

NATIONAL AERONAUTICS AND SPACE ADMINISTRATION

For sale by the Clearinghouse for Federal Scientific and Technical Information
Springfield, Virginia 22151 – Price $3.00

ABSTRACT

The method of applying geometrical optics techniques to diffraction by antennas and scattering bodies is outlined. The basic technique employs diffraction by a conducting wedge, and may be applied to antennas and scatterers which can be modeled from wedges. This method is an extension of the Geometrical Theory of Diffraction[1, 2].

Three formulations of the solution to wedge diffraction are used for various conditions of application. The basic characteristics of each formulation is discussed. The method is discussed in detail by application to calculation of the radiation patterns of parallel-plate waveguides. The treatment of radiation patterns of pyramidal horn antennas and rectangular waveguides, and diffraction by thick walls is outlined. The application of this method to analytical determination of gain, effective aperture, and aperture admittance of parallel-plate guides and coupling between guides is discussed.

TABLE OF CONTENTS

I. INTRODUCTION

The purpose of this presentation is an organized outline of the geometrical optics techniques for diffraction which are available for antenna analysis. The principal tool employed is diffraction by a conducting wedge; the resulting electromagnetic field may be treated as the superposition of the geometrical optics field and the diffracted field which behaves as a cylindrical wave radiating from the edge of the wedge. Thus the techniques of ray optics can be used with which the field can be determined from the diffracted rays from the edge and the geometrical optics rays. The values of the diffracted rays are determined from the canonical solution to wedge diffraction.

The method employed is an extension of the Geometrical Theory of Diffraction[1, 2]. Previously only plane wave diffraction coefficients were used in the Geometrical Theory of Diffraction; however, the use of diffraction by cylindrical waves has been found necessary in the treatment of antennas. Consequently, different formulations of wedge diffraction have been substituted for the plane wave diffraction coefficients.

Three formulations of the solution to wedge diffraction are employed. Two of these formulations may be used for diffraction by either a plane wave or a cylindrical wave; for plane wave diffraction the field may be obtained for observation points at any distance from the edge whereas for cylindrical wave diffraction the distance of any observation point from the edge must be large compared to that of the source. The formulation of Pauli[3] is convenient to use for cases in which the distance parameter is greater than a wavelength. The formulation in terms of cylindrical wave functions is convenient to use where the distance parameter is less than a wavelength. The third formulation is expressed in terms of finite distances to both the observation and source points.

These techniques may be applied to any two-dimensional antenna or scattering body which may be constructed from a set of wedges; the radiation or scattering pattern may be obtained for any excitation which can be expressed in terms of plane or cylindrical waves by superposition of the individual wedge diffractions. Some elementary examples include parallel-plate waveguides, walls of finite thickness, principal-plane patterns of pyramidal horn antennas, and polygonal cylinders.

A basic feature of this technique is that it does not require an assumption of the value of the total field or currents on some surface, as do conventional methods of aperture integration which employ the approximation of physical optics. This feature thus allows more accurate treatment of problems than ordinarily obtained; it also provides knowledge of the fields in terms of the incident field, thus resulting in the ability to analytically determine admittance and gain of antennas, and mutual coupling between antennas.

The geometrical ray techniques of this method provide conceptual simplicity with which solutions may be formulated. This together with superposition of wedges allows structural aspects to be taken into account, e. g., antennas mounted with and without ground planes, structures with thin or thick walls, and arbitrary waveguide truncations can be treated. In addition the fields in all space can be determined, allowing backlobe regions to be treated.

II. PLANE WAVE DIFFRACTION

A. Pauli's Formulation

The problem of straight edge diffraction by a perfectly conducting wedge was first solved by Sommerfeld[5]. He considered a plane electromagnetic wave normally incident on a wedge of angle $(2-n)\pi$ as shown in Fig. 1. Cylindrical coordinates are employed with the z-axis coincident with the edge and consequently normal to the plane of diffraction. The z-component of the total field at observation point $P(r, \psi)$ may be represented by the scalar function u, given by

$$u(r, \psi) = v(r, \psi-\psi_o) \pm v(r, \psi + \psi_o) \quad . \tag{1}$$

The minus sign applies for the boundary condition $u = 0$ on the wedge surface; thus the solution is then valid for the electric field oriented in the z-direction (polarization parallel to the edge). The plus sign applies for the normal derivative of $u = 0$ on the wedge surface, or the magnetic field oriented in the z-direction (polarization perpendicular to the edge). The quantities $v(r,\phi)$ represent the separation of the solution into incident and reflected waves and are given by

$$v(r, \phi) = v^{*}(r, \phi) + v_B(r, \phi) \tag{2}$$

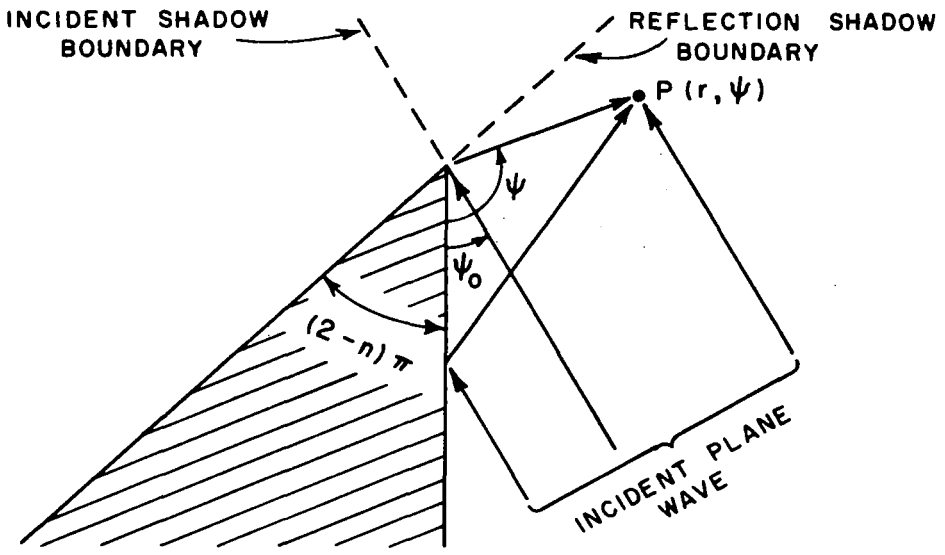

Fig. 1. Diffraction of a plane wave by a conducting wedge.

where v^* is the geometrical optics wave which is given by

$$(3) \qquad v^*(r,\phi) = \begin{cases} \exp\left[jkr\cos(\phi + 2\pi n N)\right], & \text{if } -\pi < \phi + 2\pi n N < \pi \\ & \text{for } N = 0, \pm 1, \pm 2 \ldots \\ 0, \text{ otherwise} \quad . \end{cases}$$

It is apparent from Eq. (3) that $\phi = \psi - \psi_o$ yields the incident geometrical optics wave, which consists of the incident plane wave in the illuminated region ($0 < \psi < \pi + \psi_o$) and is zero in the shadow region ($\pi + \psi_o < \psi < \pi n$). The two regions are separated by the incident shadow boundary as shown in Fig. 1, at which the discontinuity in the geometrical optics wave occurs. Similarly, the reflected geometrical optics wave is given by Eq. (3) for $\phi = \psi + \psi_o$; it consists of the plane wave reflected by the wedge in the illuminated region ($0 < \psi < \pi - \psi_o$) and is zero in the shadow region ($\pi - \psi_o < \psi < \pi n$). The two regions for the reflected wave are separated by the reflection shadow boundary at $\psi = \pi - \psi_o$. As seen from Eq. (2) each geometrical optics wave has an associated diffracted wave $v_B(r,\phi)$. The diffracted waves describe the diffraction effect of the edge for finite wavelengths; each diffracted wave combines with the respective geometrical optics wave to eliminate the discontinuity at the appropriate shadow boundary.

The separation of Eq. (1) into incident and reflected waves is a natural form of the solution and allows the diffracted wave $v_B(r,\phi)$ to be conveniently treated for computations. Pauli[3] obtained a practical formulation for the diffracted wave $v_B(r,\phi)$ for a wedge of angle $(2-n)\pi$ which is given by

$$(4) \qquad v_B(r,\phi) = \frac{2e^{j\frac{\pi}{4}}}{\sqrt{\pi}} \left(\frac{1}{n} \sin\frac{\pi}{n}\right) \frac{\left|\cos\frac{\phi}{2}\right|}{\cos\frac{\pi}{n} - \cos\phi/n}$$

$$\cdot\, e^{jkr\cos\phi} \int_{\sqrt{kr(1+\cos\phi)}}^{\infty} e^{-j\tau^2}\, d\tau + [\text{Higher Order Terms}]$$

where the higher order terms are negligible for large r.

Oberhettinger[6] has obtained a similar series form for v_B in which the leading term is identical to the Fresnel integral form for half-plane diffraction, i. e., the same as the leading term in Eq. (4) with n = 2. From the computational aspect Pauli's form is more convenient to apply to the general wedge because of the inclusion of the dependence on wedge angle in the leading term.

In summary, the total field for a plane wave incident on a perfectly conducting wedge is given by

$$(5) \qquad u(r,\psi) = \left\{ \begin{matrix} \exp[jkr\cos(\psi-\psi_o)] \\ 0 \end{matrix} \right\} \pm \left\{ \begin{matrix} \exp[jkr\cos(\psi+\psi_o)] \\ 0 \end{matrix} \right\}$$

$$+ v_B(r,\psi-\psi_o) \pm v_B(r,\psi+\psi_o)$$

where the proper choice of terms in the brackets are determined from Eq. (3) and the choice of the sign ($\pm$) is determined by the polarization. The last two terms, the diffracted waves, are correspondent to the incident and reflected geometrical optics terms, respectively; each term compensates the discontinuity at the shadow boundary of the respective geometrical optics term. The value of the diffracted wave on the shadow boundary is expressed by

(6) $$v_B(r,\pi) = \mp \tfrac{1}{2} e^{-jkr} + [0(r^{-\frac{1}{2}})] \begin{cases} \text{upper sign for } \phi = \pi - \\ \text{lower sign for } \phi = \pi + \end{cases} .$$

The value of $v^* + v_B$ on the shadow boundary is thus obtained as

(7) $$v^*(r,\pi) + v_B(r,\pi) = \tfrac{1}{2} e^{-jkr} + [0(r^{-\frac{1}{2}})]$$

which for large r is one-half of the incident field on the illuminated side of the shadow boundary. Each term of Eq. (5) individually satisfies the wave equation. The diffracted terms, incident and reflected, combine to fulfill the boundary conditions as do the geometrical optics terms.

For large values of $kr(1 + \cos\phi)$, Eq. (4) may be approximated as

(8) $$v_B(r,\phi) = \frac{e^{-j(kr+\pi/4)}}{\sqrt{2\pi kr}} \quad \frac{\frac{1}{n} \sin\frac{\pi}{n}}{\cos\frac{\pi}{n} - \cos\frac{\phi}{n}} = D(\phi) \frac{e^{-jkr}}{\sqrt{r}} .$$

The diffracted field as expressed by Eq. (8) is that from which the asymptotic diffraction coefficients $D(\phi)$ of the Geometrical Theory of Diffraction[1, 2] are obtained. It is evident from Eq. (8) that the diffracted field, when observed sufficiently far from the edge and sufficiently removed from the shadow boundary, appears to be a directional cylindrical wave radiating from the edge. It is this property which allows the diffraction effect of the edge to be treated by geometrical optics techniques.

The exact function $v(r,\phi)$ is periodic in $2\pi n$ so that

(9) $$v(r, \phi + 2\pi n N) = v(r,\phi), \quad N = 0, \pm 1, \pm 2 \ldots$$

However, the Fresnel integral term of v_B does not satisfy this periodicity property for $n \neq 2$; moreover, the series representation of v_B given in Eq. (4) diverges for the shadow boundary values

(10) $$\phi = \pm \pi + 2\pi n N, \quad n \neq 2, \quad N = \pm 1, \pm 2 \ldots$$

Near the values of ϕ given in Eq. (10) the series representation of v_B converges slowly, but the periodicity property of the exact function $v(r, \phi)$ may be used to overcome convergence difficulties near these values. For example, if v_B is to be evaluated for ϕ near $2\pi n - \pi$, the following substitution may be made to yield readily calculated values:

$$v_B(r, \phi) \rightarrow v_B(r, \phi - 2\pi n) \quad . \tag{11}$$

The only case for which all boundaries are regular and the substitution of Eq. (11) is not necessary is for the thin half-plane. In this case, for which $n = 2$, the higher order terms of Eq. (4) are identically zero; and the Fresnel integral term yields the exact v_B.

A frequently encountered example of divergence is illustrated in Fig. 2 in which the incident wave illuminates both sides of a wedge. In this example the reflected wave has two shadow boundaries for which values of the angular argument $\phi = \psi + \psi_o$ are

$$\begin{aligned} &\phi_1 = \pi, \quad \psi_1 = \pi - \psi_o \\ &\phi_2 = 2n\pi - \pi, \quad \psi_2 = 2n\pi - \pi - \psi_o \end{aligned} \quad . \tag{12}$$

For values of ϕ near $\phi_2 = 2n\pi - \pi$ the substitution of Eq. (11) may be used for practical computation of v_B.

The solution as expressed in Eq. (5) exists on a Riemann surface of two sheets, each sheet of angular extent πn. If the angles ψ and ψ_o are measured from one wedge surface, the physical space of the solution corresponds to the sheet on which

$$2\pi n N \leq \psi \leq \pi n + 2\pi n N, \quad N = 0, \pm 1, \pm 2 \ldots$$

In computations the physical space is ordinarily taken as $0 \leq \psi \leq \pi n$ with the caution that ψ not lie outside this interval.

For grazing incidence ($\psi_o = 0$), the reflected and incident terms combine mathematically to give the solution corresponding to the incident wave $2 \exp(jkr \cos \psi)$. In computations it is important to note that the formulation for this case does not correspond to a unit-amplitude incident wave;

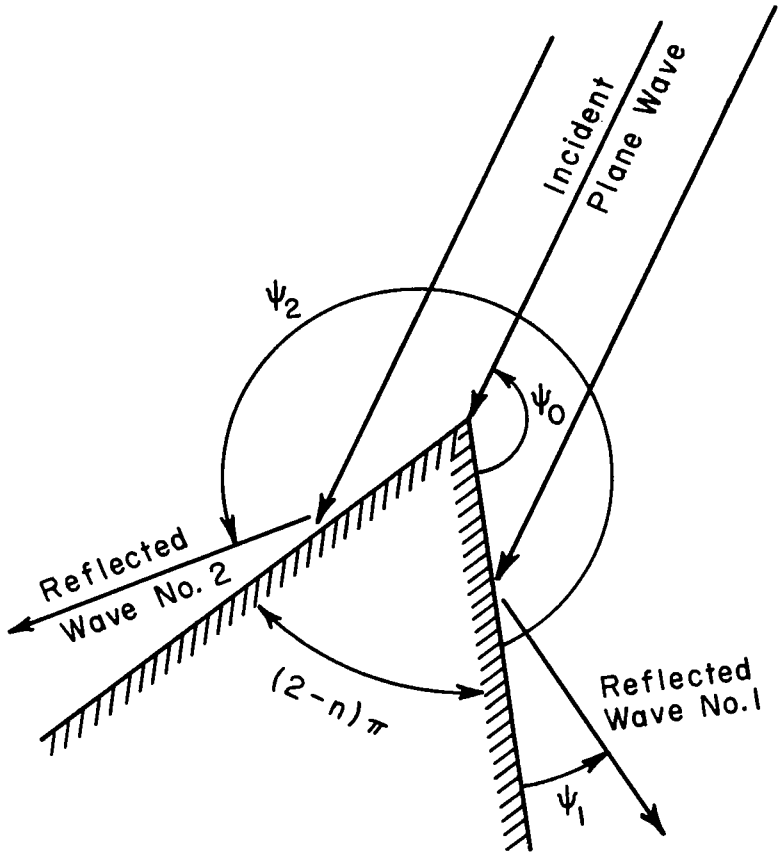

Fig. 2. Reflection from both wedge surfaces.

and a convenient way to treat grazing incidence is to use

$$v(r,\psi) = \begin{cases} \exp(jkr\cos\psi) \\ o \end{cases} + v_B(r,\psi), \quad \psi_o = 0 \tag{13}$$

B. Cylindrical Wave Function Formulation

As previously discussed, the series expression for $v_B(r,\phi)$ for a finite wedge angle contains higher order terms which are generally negligible for r large compared to the wavelength. However, computation is

difficult for $r < \lambda$ because the higher order terms are not well formulated and are unwieldy. A more suitable means for computing $v_B(r,\phi)$ for $r < \lambda$ can be obtained from the Green's function form of the solution given by[7]

$$(14) \qquad v_B(r,\phi) = \frac{1}{n} \sum_{m=0,\,1}^{\infty} \epsilon_{\frac{m}{n}} j^{\frac{m}{n}} J_{\frac{m}{n}}(kr) \cos \frac{m}{n}\phi - v^*(r,\phi)$$

where v^* is obtained from Eq. (3) and Neumann's number ϵ_ν is 1 for $\nu = 0$ and 2 for $\nu > 0$. For $r < \lambda$, the inclusion of the terms for which $\frac{m}{n} \leq 15$ is usually adequate; for $r > \lambda$ the Fresnel integral term of Eq. (4) is used. Although the two domains for the application of either Eq. (4) or (14) as defined by the border line $r = \lambda$ are usually satisfactory, it should be noted that for wedge angles near π ($n \approx 1$) the leading term of Eq. (4) is inaccurate even for values of $r > \lambda$ [8]. The form of Eq. (14) may be used for larger values of r when $n \approx 1$ by including more terms.

III. CYLINDRICAL WAVE DIFFRACTION

A. Far Field Form

Diffraction of a cylindrical wave by a wedge is important in diffraction problems. Since the diffraction of a plane wave by a wedge is very similar to a cylindrical wave radiating from the edge (see Eq. (8)), a subsequent diffraction of this diffracted wave may be treated as wedge diffraction with cylindrical wave incidence. The solution for cylindrical wave diffraction can be determined in several ways. The diffracted wave at large distances from the edge may be determined by the use of the principle of reciprocity together with the solution for plane wave diffraction. For plane wave incidence the total field at observation point P of cylindrical coordinates (r, ψ), as shown in Fig. 3, is given by $u(r, \psi)$ of Eq. (5). Now consider the situation in Fig. 3 in which the wedge is illuminated by a cylindrical wave with its source at (r_o, α). By reciprocity the field u_a in the direction ξ is equal to the field u_b which is located at the point $(r = r_o, \psi = \alpha)$ with a plane wave incident from the direction $\psi_o = \xi$. Thus the field at infinity for a perfectly conducting wedge illuminated by a line source at (r_o, α) is given by

$$(15) \qquad u_a(\xi) = v(r_o,\ \xi - \alpha) \pm v(r_o,\ \xi + \alpha) \quad .$$

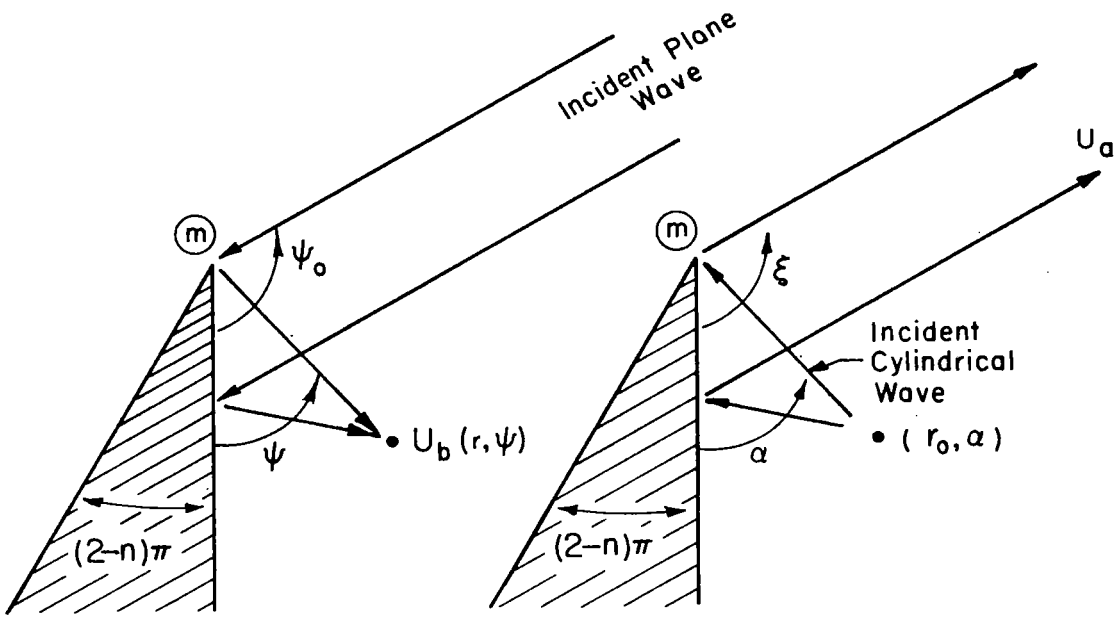

Fig. 3. Illustration of reciprocity.

Equation (15) represents the field at an infinite distance from the edge for a source whose incident field at infinity is $\exp[jkr_o\cos(\xi-\alpha)]$. However, the radial distribution of the line source and its diffraction is $\frac{e^{-jkr}}{\sqrt{r}}$.

Consequently, the total field distribution at radial distances from the edge which are large compared to the distance r_o of the line source may be expressed as

$$u = \frac{e^{-jkr}}{\sqrt{r}}\left[\begin{cases}\exp[jkr_o\cos(\psi-\psi_o)]\\ 0\end{cases}\pm\begin{cases}\exp[jkr_o\cos(\psi+\psi_o)]\\ 0\end{cases}\right.$$
$$\left. + v_B(r_o,\ \psi-\psi_o) \pm v_B(r_o,\ \psi+\psi_o)\right] . \tag{16}$$

The coordinates (r,ψ) and ψ_o are reintroduced to represent the observation point and the angle of incidence. The exponential quantities in the brackets are simply the phase factors of the incident and reflected geometrical optics waves; they arise because the phase of the solution is referred to the edge.

In regions sufficiently removed from the shadow boundary, the cylindrical wave form of v_B given in Eq. (8) may be used. Equation (8) also expresses the field at infinity for plane wave incidence. Thus the diffraction for cylindrical wave incidence is the same as that for plane wave incidence in regions sufficiently removed from the shadow boundary; the region about the boundary in which the two are significantly different depends on the radial distance r_o to the line source.

The diffraction expressed by Eq. (16) is that for a line source with an omnidirectional pattern. In the application of Eq. (16) to diffraction by a directional wave, it is assumed that the diffraction is the same as that of an omnidirectional source, with the same value of the incident field as the directional wave has in the direction of the edge. This is a valid assumption for an incident wave which has small variation relative to its magnitude near the edge.

Thus the total wave for diffraction of a directional cylindrical wave by a perfectly conducting wedge is given by

$$E = \frac{e^{-jkr}}{\sqrt{r}} \left[F(\psi) \begin{cases} \exp[jkr_o \cos(\psi - \psi_o)] \\ 0 \end{cases} \pm F(2\pi - \psi) \begin{cases} \exp[jkr_o \cos(\psi + \psi_o)] \\ 0 \end{cases} \right] + F(\pi + \psi_o) \left[v_B(r_o, \psi - \psi_o) \pm v_B(r_o, \psi + \psi_o) \right] \tag{17}$$

where $F(\psi)$ is the pattern of the line source. The coordinates of the observation point are (r, ψ) whereas those of the source are (r_o, ψ_o). Equations (16) and (17) are valid for $r \gg r_o$. The interpretation of the various terms in these equations is similar to that for plane wave incidence; the discontinuities at the shadow boundaries of the geometrical optics waves are compensated by the diffracted waves in the same manner.

B. Elements of Superposition

By superimposing conducting wedges a number of two-dimensional antennas and scattering bodies may be modeled. Some elementary examples include parallel-plate waveguides, walls of finite thickness, principal-plane cross sections of pyramidal horn antennas and polygonal cylinders. The key to determining the radiation or scattering patterns of theoretical models is the proper use of superposition of wedge diffractions. The elements of superposition which are used to obtain far field patterns will now be described.

Consider the two wedges and source S shown in Fig. 4. The pattern of source S is denoted $F(\psi)$; and hence the diffraction pattern of wedge A with source S is given by Eq. (17) with $\psi_o = \alpha_o$ and $r_o = x_o$.

The diffracted wave from wedge A is treated as that of a line source which illuminates wedge B with a wave expressed by

$$E_{BA} = \frac{e^{-jkr}}{\sqrt{r}} \left[v_B(x_o, \alpha_2 - \alpha_o, n_A) \pm v_B(x_o, \alpha_2 + \alpha_o, n_A) \right] F(\pi + \alpha_o) \tag{18}$$

where the dependence on wedge angle is noted by n_A. Thus Eq. (17) may again be used to give the diffraction from wedge B as

$$E_B = E_{BA} \left[v_B(x_1, \psi' - \alpha_1, n_B) \pm v_B(x_1, \psi' + \alpha_1, n_B) \right] \tag{19}$$

where the phase is referred to the tip of wedge B and

$$\psi' = \psi + \pi + \alpha_1 - \alpha_2 \quad . \tag{20}$$

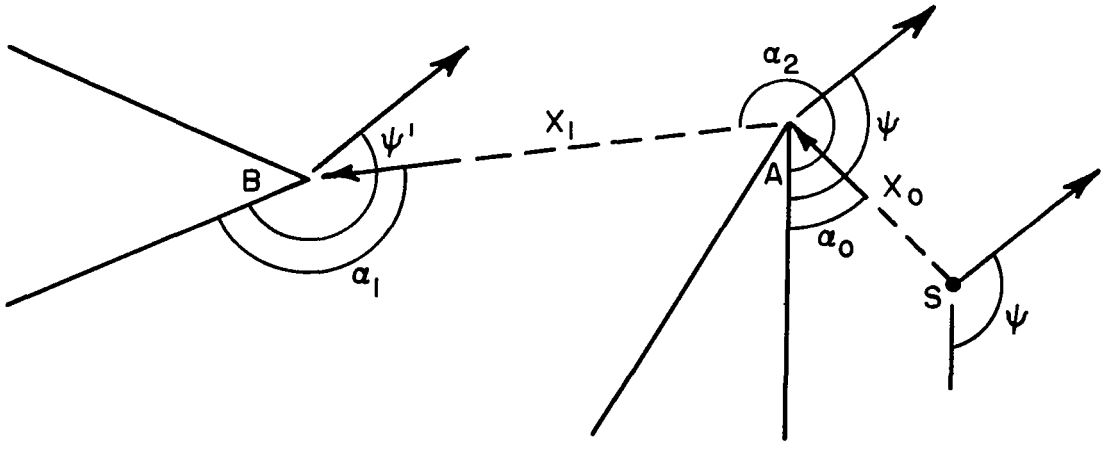

Fig. 4. Illustration of superposition.

By suppressing the cylindrical wave propagation factor $e^{-jkr}/\sqrt{r}$ the solution to the diffraction problem in Fig. 4 may be written as

$$
\begin{aligned}
(21) \qquad D_T(\psi) &= F(\psi)\, \exp\left[jkx_o \cos(\psi - \alpha_o)\right] \\
&\quad + F(\pi + \alpha_o) \left[v_B(x_o, \psi - \alpha_o, n_A) \pm v_B(x_o, \psi + \alpha_o, n_A) \right] \\
&\quad + F(\pi + \alpha_o) \left[v_B(x_o, \alpha_2 - \alpha_o, n_A) \pm v_B(x_o, \alpha_2 + \alpha_o, n_A) \right] \left[v_B(x_1, \psi' - \alpha_1, n_B) \right. \\
&\quad \left. \pm v_B(x_1, \psi' + \alpha_1, n_B) \right] \exp\left[jkx_1 \cos(\psi' - \alpha_1)\right] \quad .
\end{aligned}
$$

Each term is used only in the region for which its contribution is not shadowed by one of the wedges. In addition there are reflections of the diffracted rays from each wedge and further diffractions between the wedge tips. The last term of Eq.(21) demonstrates that superposition involves the direct multiplication of v_B quantities plus proper referral of phase (to the tip of wedge A in this example).

C. Near Field Form

The diffracted field at distances from the edge comparable to that of the source as shown in Fig. 5 may be expressed in a form used in Ref. 4 but modified to two dimensions and generalized for wedge diffraction. The resulting diffracted field is given by

$$
(22) \qquad u_d = \frac{e^{-jk(r + r_o)}}{\sqrt{r + r_o}} \; e^{jk \frac{r\, r_o}{r + r_o}} \left[v_B\left(\frac{r\, r_o}{r + r_o}, \psi - \psi_o \right) \pm v_B\left(\frac{r\, r_o}{r + r_o}, \psi + \psi_o \right) \right] \quad .
$$

The incident geometrical optics field is given by

$$
(23) \qquad u_i = \frac{e^{-jkR}}{\sqrt{R}} = \frac{e^{-jk\left(r^2 + r_o^2 - 2r\, r_o \cos(\psi - \psi_o)\right)^{\frac{1}{2}}}}{\left(r^2 + r_o^2 - 2r\, r_o \cos(\psi - \psi_o)\right)^{\frac{1}{4}}}
$$

where R is the distance from the source to the observation point. The reflected geometrical optics field is given by

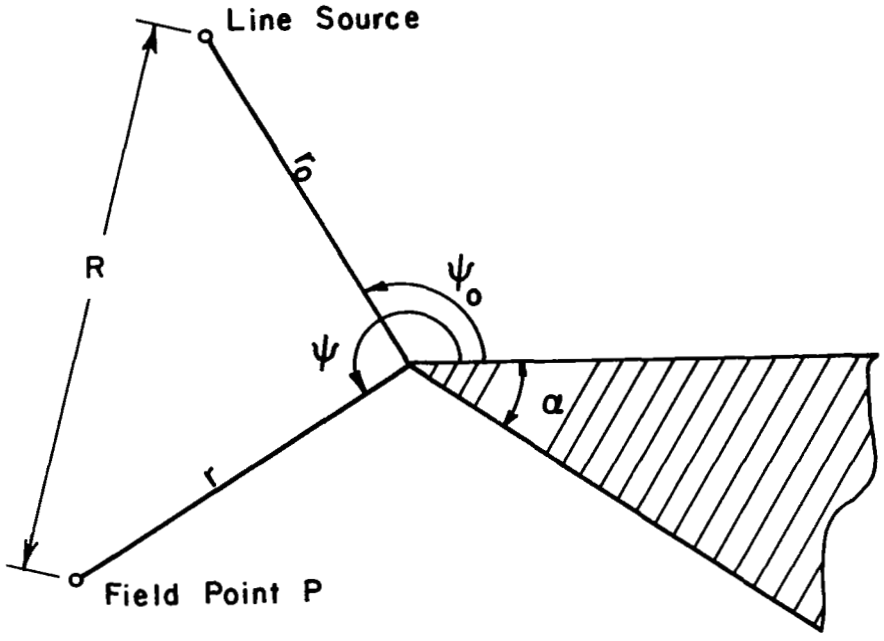

Fig. 5. Near field diffraction by wedge.

$$u_r = \pm \frac{e^{-jk\left(r^2 + r_o^2 - 2r\, r_o \cos(\psi + \psi_o)\right)^{\frac{1}{2}}}}{\left(r^2 + r_o^2 - 2r\, r_o \cos(\psi + \psi_o)\right)^{\frac{1}{4}}} \tag{24}$$

The defined regions for each geometrical optics term may be determined from Eq. (3). The sign ($\pm$) is chosen according to the polarization. For $r \gg r_o$, Eq. (22) reduces to the form given in Eq. (16).

IV. RADIATION PATTERNS OF PARALLEL-PLATE WAVEGUIDES

A. TEM Mode

The diffraction at the aperture of the parallel-plate waveguide shown in Fig. 6 is discussed in this section[9, 10]. The guide angle θ_g between the edges of the plates may be adjusted for various mounting configurations, as may the wedge angles WA1 and WA2. The TEM waveguide mode is treated first; in this mode an incident plane wave propagates parallel to the axis of the guide with polarization perpendicular to the waveguide walls as shown in Fig. 6(a).

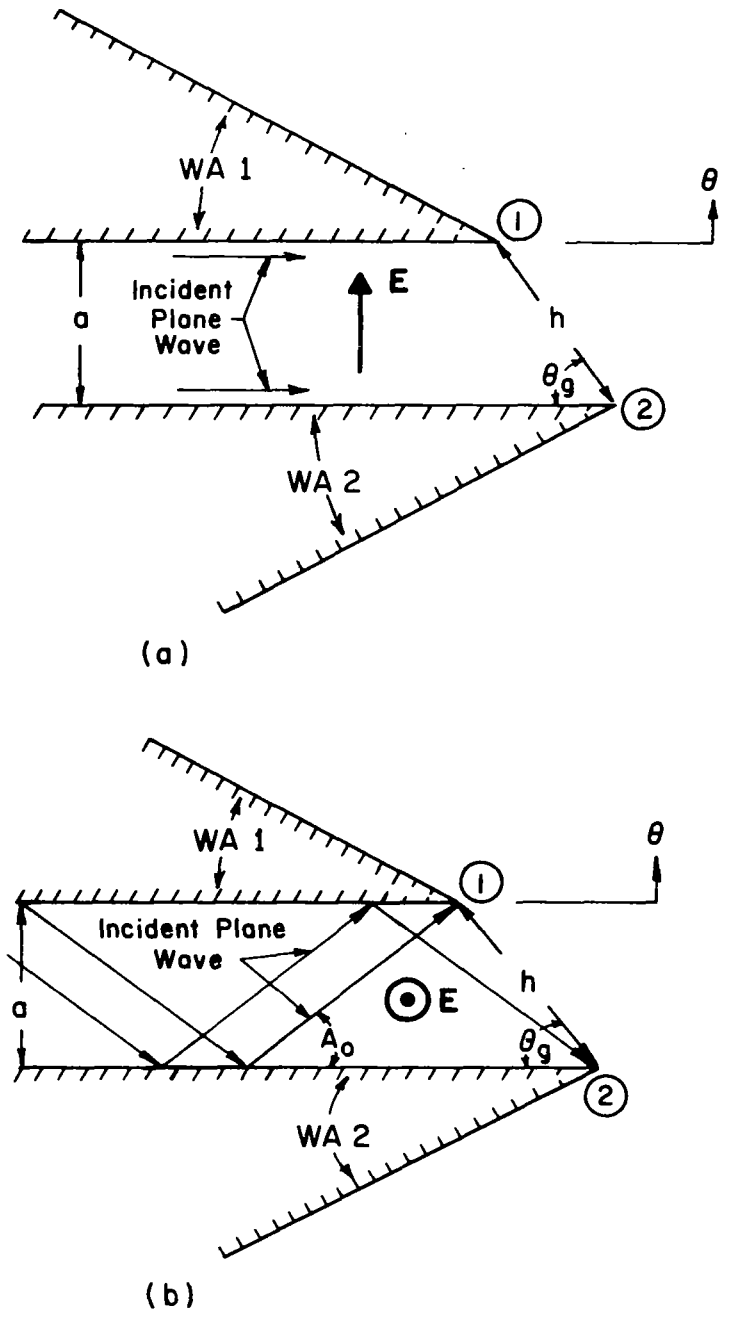

Fig. 6. TEM and TE_{01} modes in a parallel-plate waveguide.

The diffraction from the guide aperture is treated by superimposing the diffracted rays from each of the wedges. The singly diffracted wave from edge 1 is given by Eq. (8) for plane wave diffraction as

$$(25) \qquad R_{D1}(\theta) = \frac{1}{n_1} \sin\frac{\pi}{n_1}\left(\frac{1}{\cos\frac{\pi}{n_1} - \cos\frac{\pi+\theta}{n_1}}\right)$$

where the factor $\frac{e^{-j(kr+\pi/4)}}{\sqrt{2\pi kr}}$ is suppressed because only angular variations are of interest at this point. Similarly, the singly diffracted wave from edge 2 is obtained as

$$(26) \qquad R_{D2}(\theta) = \frac{1}{n_2} \sin\frac{\pi}{n_2}\, e^{-jka\cot\theta_g}\left(\frac{1}{\cos\frac{\pi}{n_2} - \cos\frac{\pi-\theta}{n_2}}\right)$$

where the factor $e^{-jka\cot\theta_g}$ represents the phase of the incident wave at edge 2.

The direction $\theta = 0$ corresponds to the direction of the geometrical optics rays. Although the individual rays R_{D1} and R_{D2} are without limit at $\theta = 0$, the limit of $(R_{D1} + R_{D2})$ as $\theta \to 0$ expresses the effect of the geometrical optics rays.

Some of the singly diffracted rays from edge 1 may be reflected from wedge 2 as seen in Fig. 7. The reflected rays are given by

$$(27) \qquad R_{RFL}(\theta) = R_{D1}(-\theta), \quad \theta_g < \theta < \pi/2 \quad .$$

Equations (25) and (26) express the diffraction of the incident waves by wedges 1 and 2, respectively. Equation (27) (the reflected wave) expresses an interaction between the two wedges. Further, the singly diffracted rays may again be diffracted producing "doubly diffracted" rays and so on to higher and higher order interactions between the two wedges. The necessity of including higher order diffraction terms becomes apparent upon close examination of Fig. 8. Figure 8 reveals that R_{D1} has a shadow boundary at $\theta = -\theta_g$, R_{D2} has a shadow boundary at $\theta = \pi - \theta_g$, and R_{RFL} has shadow boundaries at $\theta = \theta_g$ and $\theta = \pi/2$. At each shadow boundary a

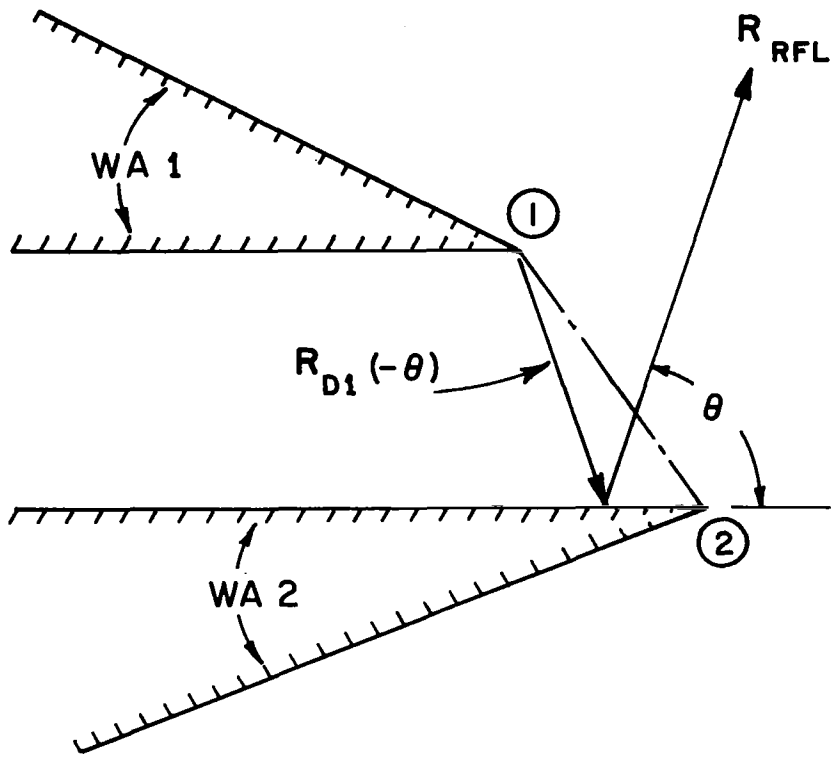

Fig. 7. Illustration of a reflected ray.

discontinuity in the respective ray is encountered. In order to eliminate these discontinuities it is necessary to take into account the doubly diffracted rays diagrammed in Fig. 9.

The singly diffracted ray R_{D1} illuminates edge 2, giving rise to the doubly diffracted ray R_{DD2}, and R_{D2} causes R_{DD1} in a similar manner*. Then the sums $(R_{D1} + R_{DD2})$ and $(R_{D2} + R_{DD1})$ will be continuous at $\theta = -\theta_g$ and $\theta = \pi - \theta_g$, respectively. In the case of the reflected term the sum $(R_{RFL} + R_{DD2})$ is continuous at $\theta = \theta_g$. The notation employed for the various rays is presented in Table I for reference:

---

* Note that the subscripts are used to trace the ray from point to point. In the case of R_{DDk} the subscript denoting the origin of the singly diffracted ray is dropped for simplicity.

TABLE I
Notation for Rays

Ray	Description	Source
R_{D1}	Singly diffracted ray from edge 1.	Incident Plane Waves
R_{D2}	Singly diffracted ray from edge 2.	Incident Plane Waves
R_{RFL}	R_{D1} reflected by wedge 2.	Incident Plane Waves
R_{D1G}	R_{D1} $(-\theta_g)$	Incident Plane Waves
R_{D1P}	R_{D1} $(-\pi/2)$	Incident Plane Waves
R_{D2G}	R_{D2} $(\pi-\theta_g)$	Incident Plane Waves
R_{DD1}	Doubly diffracted ray from edge 1.	R_{D2G}
R_{DD2}	Doubly diffracted ray from edge 2.	R_{D1G}
R_{D1RD1}	Doubly diffracted ray caused by reflection of R_{D1} from wedge 2, illuminating edge 1.	R_{D1P}
R_1	Total ray from edge 1.	
R_2	Total ray from edge 2.	
R_{1G}	$R_1(-\theta_g)$	
R_{1P}	$R_1(-\pi/2)$	
R_{2G}	$R_2(\pi-\theta_g)$	
R_{HD1}	Total higher order diffracted ray from edge 1.	R_{2G}, R_{1P}
R_{HD2}	Total higher order diffracted ray from edge 2.	R_{1G}

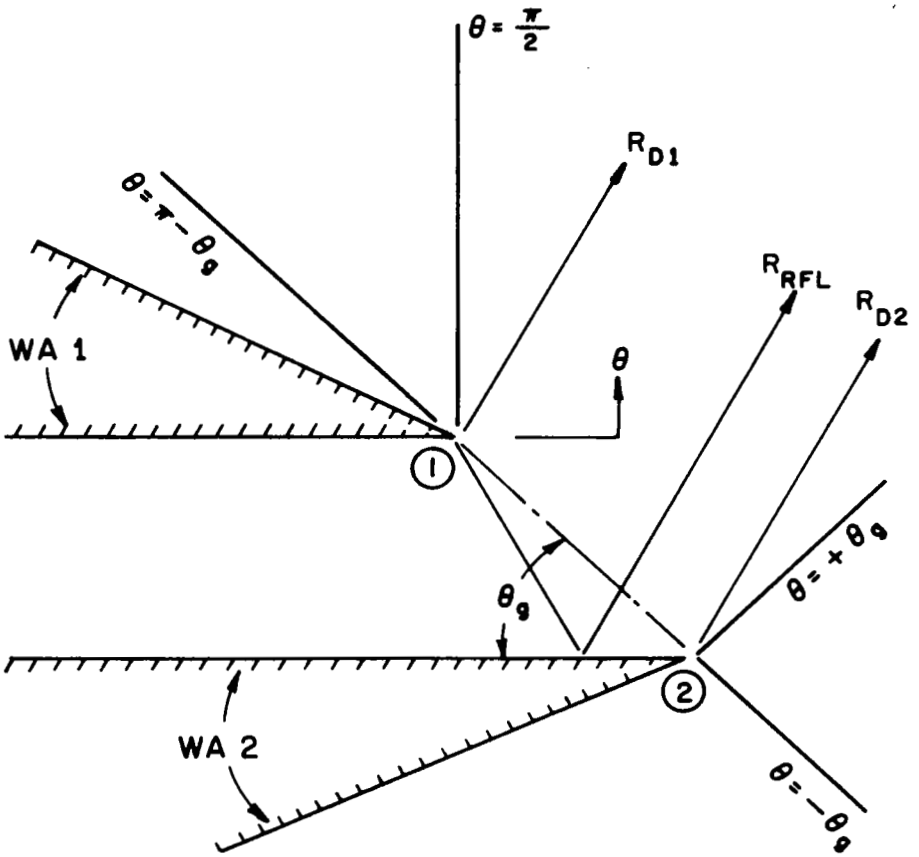

Fig. 8. Shadow boundaries of the singly diffracted and reflected rays.

The doubly diffracted rays of the general parallel-plate waveguide can be obtained by application of cylindrical wave diffraction because the singly diffracted rays cause each edge to be an apparent line source which illuminates the other edge. The doubly diffracted ray from edge 2 is obtained from Eq. (17) as

$$R_{DD2}(\theta) = R_{D1G}\left[v_B(h, \pi - \theta - \theta_g) + v_B(h, \pi - \theta + \theta_g)\right] \tag{28}$$

where

$$R_{D1G} = R_{D1}(-\theta_g) \; . \tag{29}$$

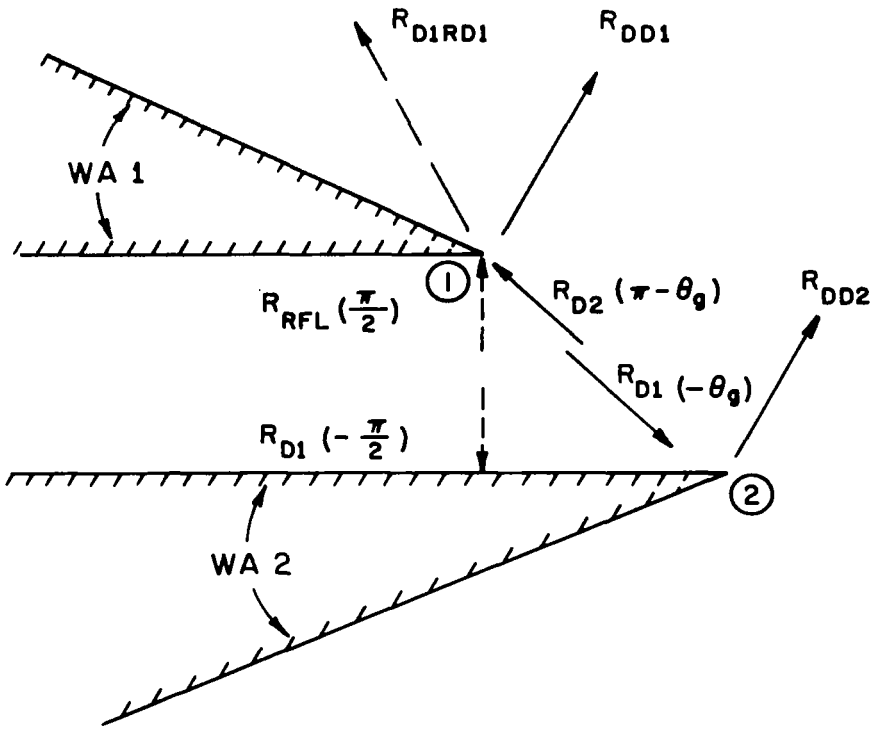

Fig. 9. Doubly-diffracted rays.

There are subsequent diffractions which result in triple and higher order diffractions from edge 2. However, the total illumination from edge 1 can be expressed as

(30) $$R_{1G} = R_1(-\theta_g)$$

where $R_1(\theta)$ is the total diffracted ray from edge 1. Consequently, the total higher order diffraction (i.e., second order and higher) from edge 2 is given by

(31) $$R_{HD2}(\theta) = R_{1G}\left[v_B(h, \pi - \theta - \theta_g) + v_B(h, \pi - \theta + \theta_g)\right].$$

Thus the total diffracted wave from edge 2 is given by

$$R_2(\theta) = R_{D2}(\theta) + R_{HD2}(\theta) \quad . \tag{32}$$

It should be noted that R_{1G} and, consequently, R_{HD2} and R_2 are unknown at this point.

In general, there are two doubly diffracted rays from edge 1. The double diffraction by the singly diffracted ray

$$R_{D2G} = R_{D2}(\pi - \theta_g) \tag{33}$$

is given by

$$R_{DD1}(\theta) = R_{D2G}[v_B(h, \theta + \theta_g) + v_B(h, 2\pi + \theta - \theta_g)] \quad . \tag{34}$$

The double diffraction by the singly diffracted ray

$$R_{D1P} = R_{D1}(-\pi/2) \tag{35}$$

is given by

$$R_{D1RD1}(\theta) = R_{D1P}\left[v_B\left(2a, \frac{\pi}{2} + \theta\right) + v_B\left(2a, \frac{3\pi}{2} + \theta\right)\right] \quad . \tag{36}$$

The total higher order illumination of edge 1 is given by

$$R_{2G} = R_2(\pi - \theta_g) \tag{37}$$

and

$$R_{1P} = R_1(-\pi/2) \quad . \tag{38}$$

Thus the total higher order diffraction from edge 1 is given by

(39) $$R_{HD1}(\theta) = R_{2G}[v_B(h, \theta + \theta_g) + v_B(h, 2\pi + \theta - \theta_g)]$$

$$+ R_{1P}\left[v_B\left(2a, \frac{\pi}{2} + \theta\right) + v_B\left(2a, \frac{3\pi}{2} + \theta\right)\right] .$$

Consequently, the total diffraction from edge 1 is given by

(40) $$R_1(\theta) = R_{D1}(\theta) + R_{HD1}(\theta) \quad .$$

The diffracted waves from edges 1 and 2 are given in terms of the unknown illuminating rays R_{1G}, R_{2G} and R_{1P}. However, these rays can be determined by the solution of three simultaneous linear equations formed by expressing each unknown ray in terms of Eq. (32) or Eq. (40):

(41) $$R_{1G} = R_{D1G} + R_{2G}V_{2G}(-\theta_g) + R_{1P}\,V_{1P}(-\theta_g)$$

$$R_{1P} = R_{D1P} + R_{2G}\,V_{2G}(-\pi/2) + R_{1P}\,V_{1P}\,(-\pi/2)$$

$$R_{2G} = R_{D2G} + R_{1G}\,V_{1G}\,(\pi - \theta_g)$$

where the quantities V_{1G}, V_{1P} and V_{2G} are the unit-wave diffractions used in Eqs. (31) and (39).

The total diffracted wave from the aperture may be expressed as the superposition of the total diffracted rays from edges 1 and 2 plus the total reflected ray to yield

(42) $$R_T(\theta) = R_1(\theta) + R_2(\theta)\, e^{jkh \cos(\theta + \theta_g)}$$

$$+ R_1(-\theta)\, e^{-j2ka \sin\theta_g \sin\theta} \quad .$$

Each term in Eq. (42) contributes to the radiation pattern only in certain regions as follows:

(43)
$$R_1(\theta) : -\theta_g < \theta < \pi - W_{A1}$$
$$R_2(\theta) : \pi + W_{A2} < \theta < \pi - \theta_g$$
$$R_1(-\theta) : -\theta_g < \theta < \pi/2 \quad .$$

The exponential factors refer each term to a common phase reference at edge 1.

For the case in which $\theta_g = 90°$, no reflected rays contribute to the radiation pattern and

(44)
$$R_{1P} = 0 \text{ , for } \theta_g = 90° \quad .$$

In this case there are only two unknown rays R_{1G} and R_{2G}; and the simultaneous equations are

(45)
$$\theta_g = 90° :$$
$$R_{1G} = R_{D1G} + R_{2G}\, V_{2G}(-\pi/2)$$
$$R_{2G} = R_{D2G} + R_{1G}\, V_{1G}\left(\frac{\pi}{2}\right) \quad .$$

The total pattern for the $\theta_g = 90°$ case is given by

(46)
$$\theta_g = 90° :$$
$$R_T(\theta) = R_1(\theta) + R_2(\theta)\, e^{-jka \sin\theta}$$

where the appropriate regions for the respective terms are

(47)
$$R_1(\theta) : -\pi/2 < \theta < \pi$$
$$R_2(\theta) : -\pi < \theta < \pi/2 \quad .$$

B. TE_{01} Mode

The diffraction at the aperture of the parallel-plate waveguide for the TE_{01} mode may be treated in a similar manner as the TEM mode. The TE_{01} mode may be represented by a plane wave reflecting back and forth between the waveguide walls as shown in Fig. 6(b)[11]. The wave has a polarization parallel to the edges of the wedges which form the waveguide walls; and the angle A_o of reflection between the walls is given by

$$A_o = \sin^{-1} \frac{\lambda}{2a} \tag{48}$$

where a is the guide width. Examination of Fig. 6(b) reveals that two cases must be distinguished, as determined by

Case I : $A_o > \theta_g$

Case II : $A_o \leq \theta_g$.

Case I corresponds to the situation in which edge 2 is not illuminated by the incident plane wave. Thus, for Case I no singly diffracted ray emanates from edge 2. For Case II both edges are illuminated by the incident wave; hence singly diffracted rays emanate from both edges.

Since the polarization is parallel for the TE_{01} mode the sign $(\pm)$ in the diffraction formula is chosen as negative; and the scalar function corresponds to the electric field. The singly diffracted ray from edge 1 is obtained from Eq. (8) as

$$R_{D1}(\theta) = \frac{1}{n_1} \sin \frac{\pi}{n_1} \left[\frac{1}{\cos \frac{\pi}{n_1} - \cos \frac{\pi + \theta - A_o}{n_1}} - \frac{1}{\cos \frac{\pi}{n_1} - \cos \frac{\pi + \theta + A_o}{n_1}} \right] . \tag{49}$$

For Case II ($A_o \leq \theta_g$) the singly diffracted ray from edge 2 is given by

$$R_{D2}(\theta) = \frac{1}{n_2} \sin \frac{\pi}{n_2} \, e^{-jka[\cos \theta_g \cos A_o]} \cdot \left[\frac{1}{\cos \frac{\pi}{n_2} - \cos \frac{\pi - \theta - A_o}{n_2}} - \frac{1}{\cos \frac{\pi}{n_2} - \cos \frac{\pi - \theta + A_o}{n_2}} \right] \tag{50}$$

where the exponential factor and minus sign represent the phase of the incident plane wave at edge 2. The reflected rays are given by

$$R_{RFL}(\theta) = - R_{D1}(-\theta) \ , \ \theta_g < \theta < \pi/2 \tag{51}$$

where the preceding minus sign results from the reflection.

Multiple diffractions occur in the same manner as for the TEM mode but with the minus sign chosen in Eq. (17). Thus the total higher order diffracted waves from edges 1 and 2 for the TE_{01} mode are given by

$$R_{HD1}(\theta) = R_{2G} \left[v_B(h, \theta + \theta_g) - v_B(h, 2\pi + \theta - \theta_g) \right] - R_{1P} \left[v_B\left(2a, \frac{\pi}{2} + \theta\right) - v_B\left(2a, \frac{3\pi}{2} + \theta\right) \right] \tag{52}$$

and

$$R_{HD2}(\theta) = R_{1G} \left[v_B(h, \pi - \theta - \theta_g) - v_B(h, \pi - \theta + \theta_g) \right] \ . \tag{53}$$

The minus sign preceding R_{1P} results in the same manner as for the reflected rays of Eq. (51). The total wave from each edge is obtained by using the TE_{01} rays in the same equations valid for the TEM mode, i.e., Eqs. (32) and (40) through (47). The unknown illuminating rays are determined in the same manner as with the TEM mode by using the formulations for R_{D1}, R_{D2}, R_{HD1}, and R_{HD2} given above for the TE_{01} mode.

Patterns calculated by these equations have been found to be in good agreement with measured patterns over a wide range of guide angles (θ_g), for both TEM and TE_{01} modes[9, 10]. Typical results are shown in Figs. 10 and 11 for the TEM and TE_{01} modes, respectively. One limitation on these equations occurs for guides in which the angle A_o of the incident wave is nearly equal to the guide angle θ_g. For such guides the higher order diffracted waves from edge 2 cannot be accurately approximated by the diffraction of a uniform incident wave.

The concept of total higher order diffraction in which the total illumination of each edge can be determined from a set of simultaneous equations may be applied to any problem which can be treated by the techniques

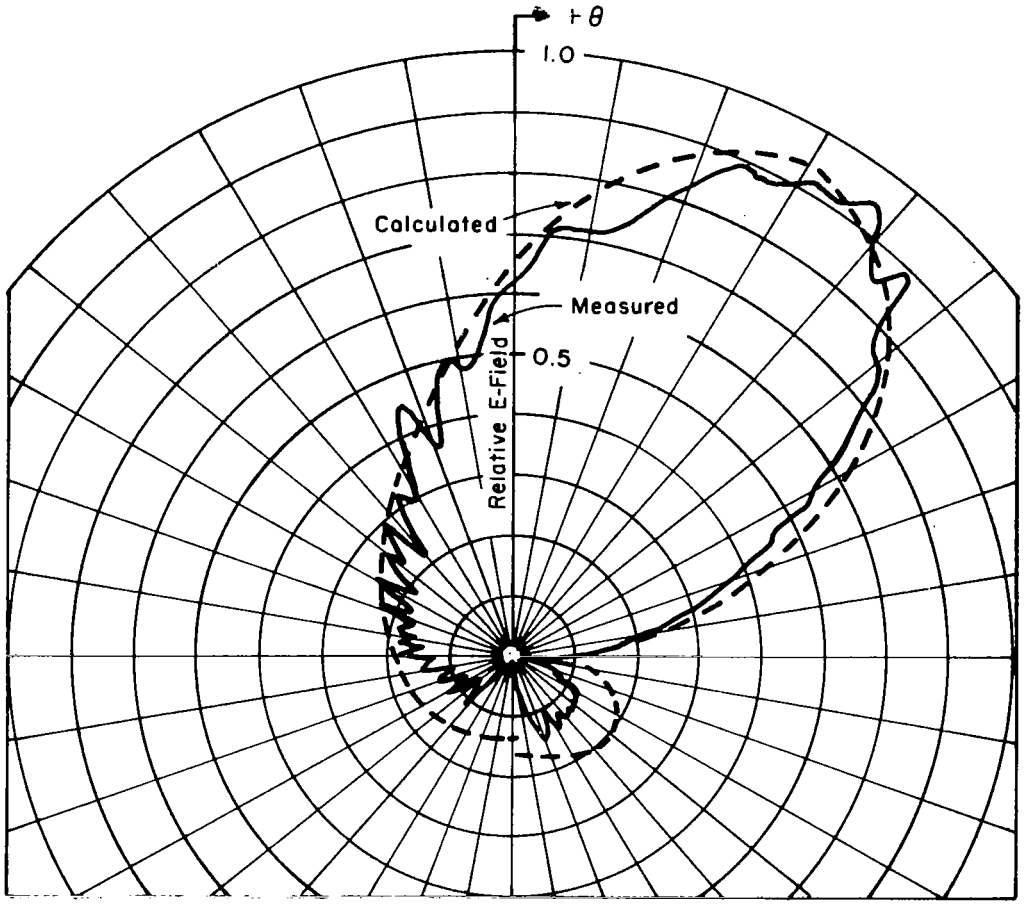

Fig. 10. Radiation pattern for TEM guide ($\theta_g = 30°$, $n_1 = n_2 = 2$, $a/\lambda = 0.424$).

discussed here. This concept provides for simpler formulation of a problem compared to the use of iteration to obtain double, triple and higher order diffractions. Because orders of diffraction higher than triple are somewhat impractical to include in computations this concept allows practical computation of problems in which dimensions are very small and, consequently, interactions are very large.

It should be noted, however, that there are limitations on applying these techniques to cases in which small dimensions are involved. In any case in which dimensions on the order of $\lambda/4$ or less are involved, careful consideration must be given to the assumption of edge diffraction being a local effect. Also the assumption that diffraction is the same as that for a uniform incident wave is not always valid - particularly for small

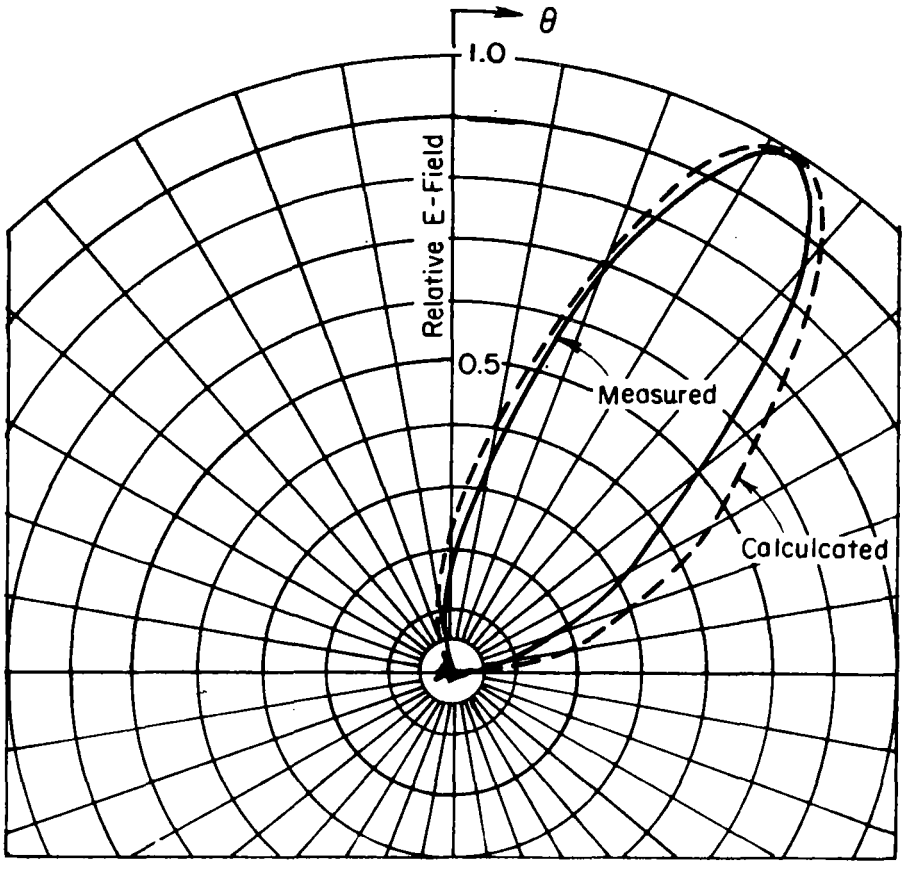

Fig. 11. Radiation pattern for TE_{01} guide ($\theta_g = 15°$, $n_1 = n_2 = 2$, $a/\lambda = 0.762$).

dimensions. In the case of the parallel-plate waveguide the higher order diffracted rays are not accurately given in all regions for cases in which the direction A_o of the incident wave is near the guide angle θ_g ; this effect is accented for small waveguides.

V. APPLICATION TO APERTURE ANTENNAS

A. E-Plane Pattern of Horn

The radiation patterns of pyramidal horn antennas have been treated in detail in Refs. 12, 13, and 14. The cross section in a principal plane for the waveguide-fed horn is shown in Fig. 12. The E-plane pattern may be closely approximated by the radiation pattern of the corner reflector shown in Fig. 13. In this model the excitation by the waveguide is approximated by a magnetic line source located at the apex of the reflector.

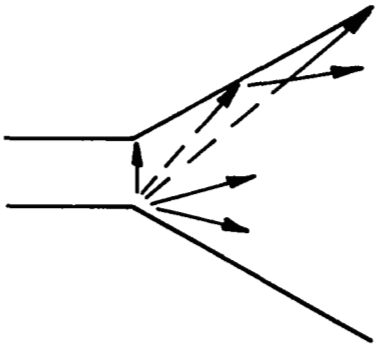

Fig. 12.

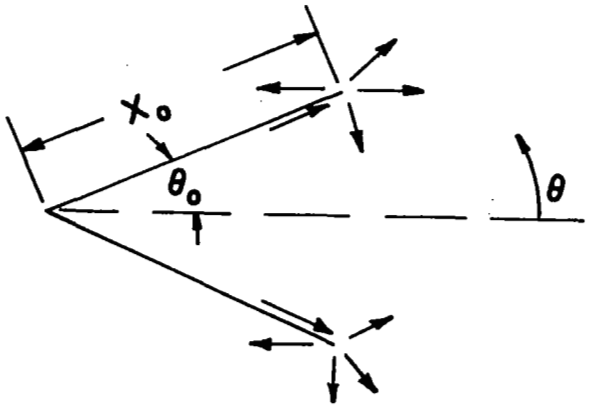

Fig. 13.

Fig. 12. Principal-plane cross section of horn.

Fig. 13. Corner reflector model for E-plane.

Initially, only the first order of diffraction was taken into account[12]. In this model the geometrical optics wave in the far field may be approximated as

$$v_G = \frac{e^{-jkr}}{\sqrt{r}} \exp\left[jkx_o \cos(\pi - \theta_o + \theta)\right], \quad -\theta_o < \theta < \theta_o \tag{54}$$

where r is measured from the top edge. The diffraction from each edge of the aperture may be obtained by straight forward application of Eq. (16). However, the reflected terms, which involve $\psi + \psi_o$, are ignored because $\psi_o = 0$ (see Eq. (13)). Hence the E-plane radiation pattern using first order diffraction is given by

$$u_E = \frac{e^{-jkr}}{\sqrt{r}} \left[\begin{cases} \exp\left[jkx_o \cos(\pi - \theta_o + \theta)\right] \\ 0 \end{cases} + v_B(x_o, \pi - \theta_o + \theta) \right. \tag{55}$$

$$\left. + \exp\left[-j2kx_o \sin\theta_o \sin\theta\right] v_B(x_o, \pi - \theta_o - \theta) \right]$$

where the exponential factor of the last term refers the phase to the upper edge. In each region specified by $\frac{\pi}{2} < |\theta| < \pi - \theta_o$, the diffracted rays from one edge are reflected by the opposite horn wall.

For horns of small dimensions, reflections and higher order diffractions must also be taken into account. The singly diffracted rays from the aperture edges which are reflected by the horn walls may be reflected several times as shown in Fig. 14. These reflections may be treated by image theory. Each image also illuminates one of the aperture edges causing further diffractions. Moreover, the diffractions from each of the aperture edges illuminates the other edge. All of these interactions are discussed in Ref. 13 and patterns are calculated by including the terms which contribute significantly. The calculated patterns agree well with measured patterns, including in backlobe regions. The first order diffraction expressed by Eq. (55) gives reasonably good results for horns larger than a few wavelengths. A sample result is shown in Fig. 15 in which the patterns are calculated in both ways.

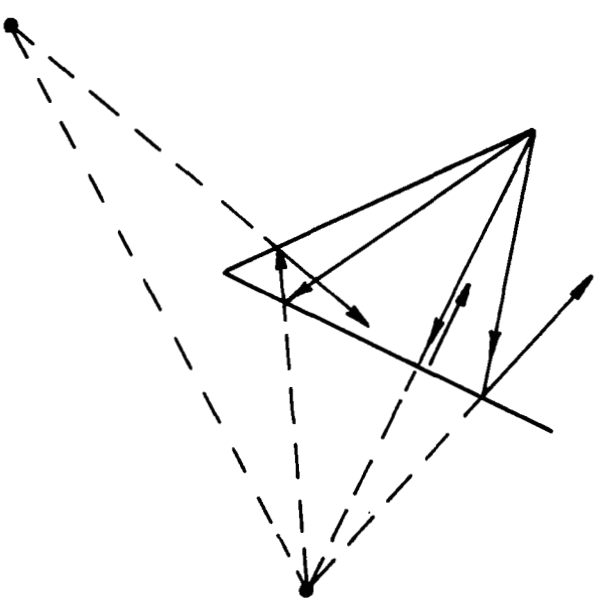

Fig. 14. Images of diffracted rays.

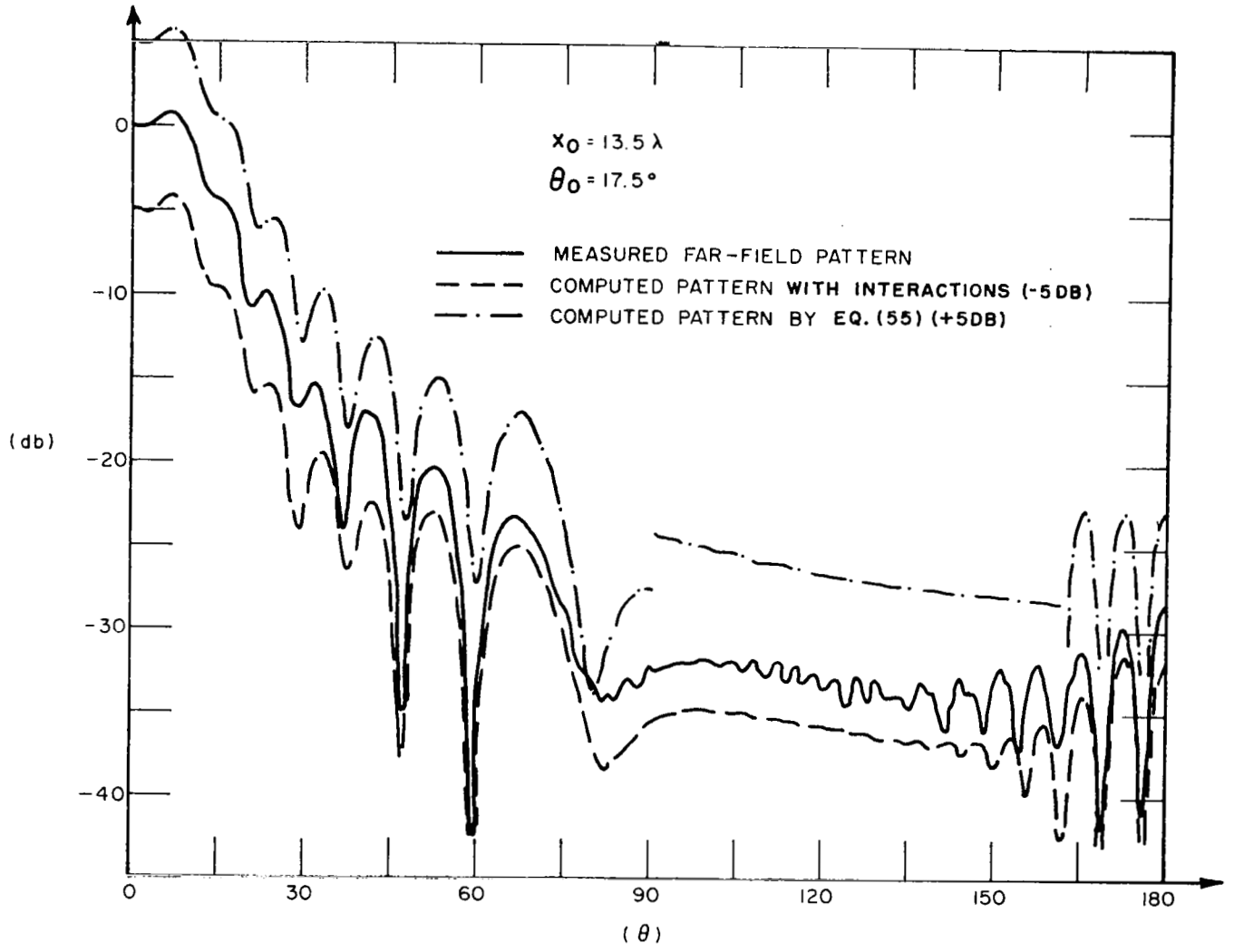

Fig. 15. E-plane patterns of horn.

B. H-Plane Pattern of Horn

The considerations for the H-plane are similar to those for the E-plane. However, the corner reflector model is not useful for H-plane patterns because the radiation from the waveguide feed cannot be approximated by a line source. The polarization properties in the H-plane require the use of an electric current line source but an electric line source located at the apex of the corner reflector will not radiate. For the H-plane the diffraction at the horn throat is treated in the same manner as a parallel-plate waveguide propagating the TE_{01} mode except that the wedge angles are larger than considered for the parallel-plate waveguide[14]. Some of the diffracted rays from each corner of the waveguide aperture are reflected by the horn walls as shown in Fig. 12. The diffracted wave from each

corner illuminates the opposite corner as well as the aperture edge of the opposite horn wall. The diffracted waves from the aperture edges produce images in the same manner as in the E-plane; and the images again illuminate the aperture edges.

In the treatment of a three-dimensional horn the diffraction from the edges of the aperture which are perpendicular to the principal E-plane, denoted E-edges, contributes significantly to radiation in the backlobe region of the H-plane. The rays incident on the E-edges result in conical diffraction because of the skew angles of incidence as shown in Fig. 16[1, 2]. Some of the resulting diffracted rays lie in the H-plane, in the sectors of angular extent slightly greater than the H-plane flare and located directly to the front and to the rear of the horn.

The contribution of these rays to the H-plane pattern may be approximated by using the assumption that the mode propagating between the horn walls has a spherical phase front with uniform amplitude in the E-plane and sinusoidal amplitude in the H-plane[15]. Thus the total ray calculated for the on-axis direction "in the H-plane" minus the diffracted rays from the H-edges of the horn aperture is taken as the value of the propagating mode in the E-plane, i.e., the total ray if the horn walls were not truncated, as indicated by dashed lines in Fig. 17(a). Thus the two surface-grazing rays in the E-plane (see Fig. 17(b)) produce two diffracted rays which coincide with the H-plane. Similarly, the other rays grazing these two surfaces produce diffracted rays in the H-plane as shown in Fig. 18; the slight disalignment between an illuminating skew ray and its diffracted ray is caused by the projection of the conical diffraction onto the H-plane. The results for a typical horn presented in Ref. 14 show the contribution

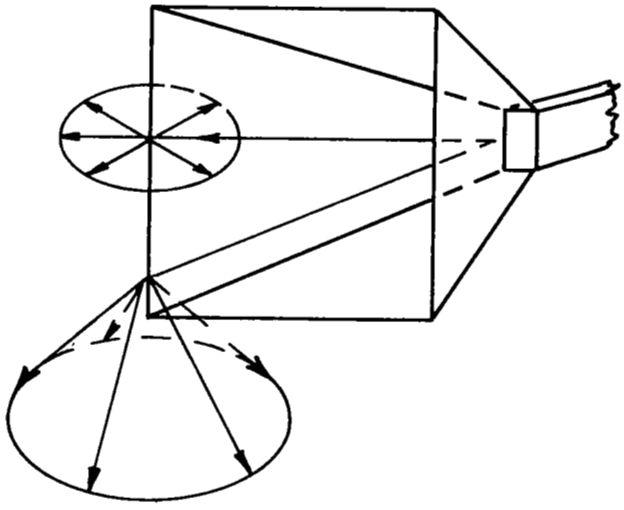

Fig. 16. Edge diffraction from pyramidal horn antenna.

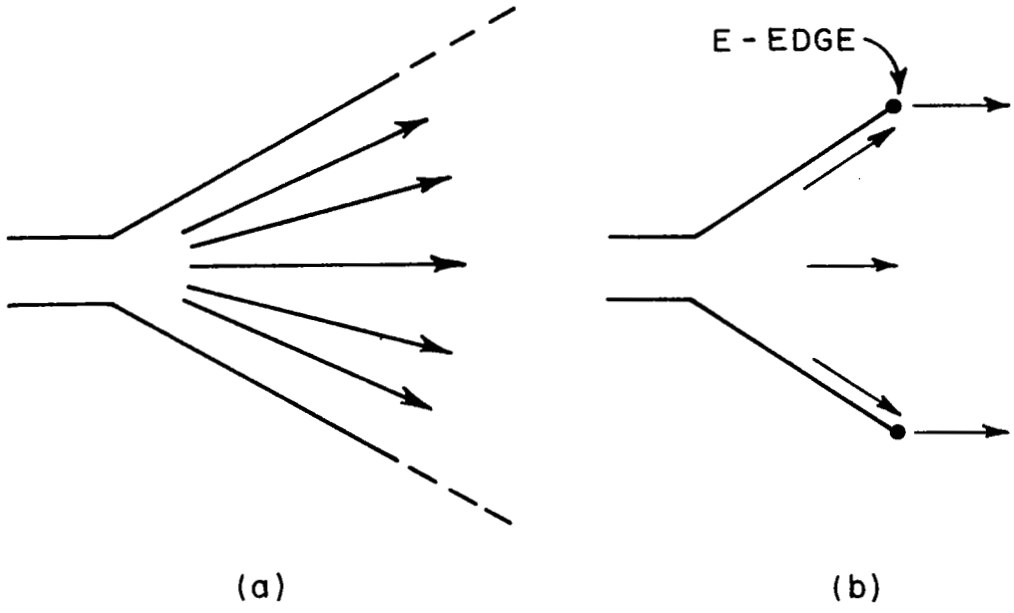

Fig. 17. E-plane cross section of horn.

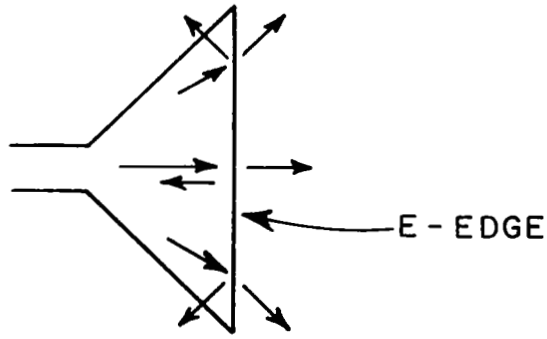

Fig. 18. Diffraction from E-edges (H-plane cross section).

from the E-edges to be negligible in the forward region; however, the E-edges are the principal contributors to the backlobe region. The H-plane pattern obtained by including the E-edge contributions to the basic H-plane diffraction was in good agreement with the measured pattern as shown in Fig. 19.

C. Diffraction by Thick Walls

The finite thickness of walls used to form waveguides or horns can be taken into account by use of these diffraction methods. The thick edge was originally modeled by two wedges as shown in Fig. 20[16]. However, plane wave diffraction coefficients were used to treat the diffraction; this is unsatisfactory for walls of small thickness because the diffraction from each corner is comparable to a cylindrical wave.

The diffraction by a rectangular edge was treated in terms of cylindrical wave diffraction in Ref. 12. For polarization perpendicular to the corners of the edge the diffraction may be formulated by the method of superposition as described in Eq. (21). The interactions between the corners may be summed in closed form by use of geometric series summation. The resulting diffracted waves for a unit-amplitude incident wave are given by

$$D_a = v_B(x_o, \psi - \psi_o) + v_B(x_o, \psi + \psi_o) + \left[v_B\left(x_o, \frac{3\pi}{2} - \psi_o\right) + v_B\left(x_o, \frac{3\pi}{2} + \psi_o\right) \right] \frac{v_B(d,0)\, v_B(d,\theta')}{1 - v_B^2(d,0)} \tag{56}$$

for corner a and

$$D_b = \left[v_B\left(x_o, \frac{3\pi}{2} - \psi_o\right) + v_B\left(x_o, \frac{3\pi}{2} + \psi_o\right) \right] \frac{v_B(d,\theta)}{1 - v_B^2(d,0)} \exp(-jkd\cos\theta) \tag{57}$$

for corner b, where the exponential factor refers the phase to corner a. The calculations in Ref. 12 were limited to walls thicker than $\lambda/2$ because the Fresnel integral term was used for v_B. However, the formulation of v_B in terms of Bessel functions as given in Eq. (14) allows small thicknesses to be treated.

For shaped edges involving three or more corners as illustrated in Fig. 21 the interactions may also be summed in closed form by use of the total higher order diffraction concept used in section IV; this is done in Ref. 8.

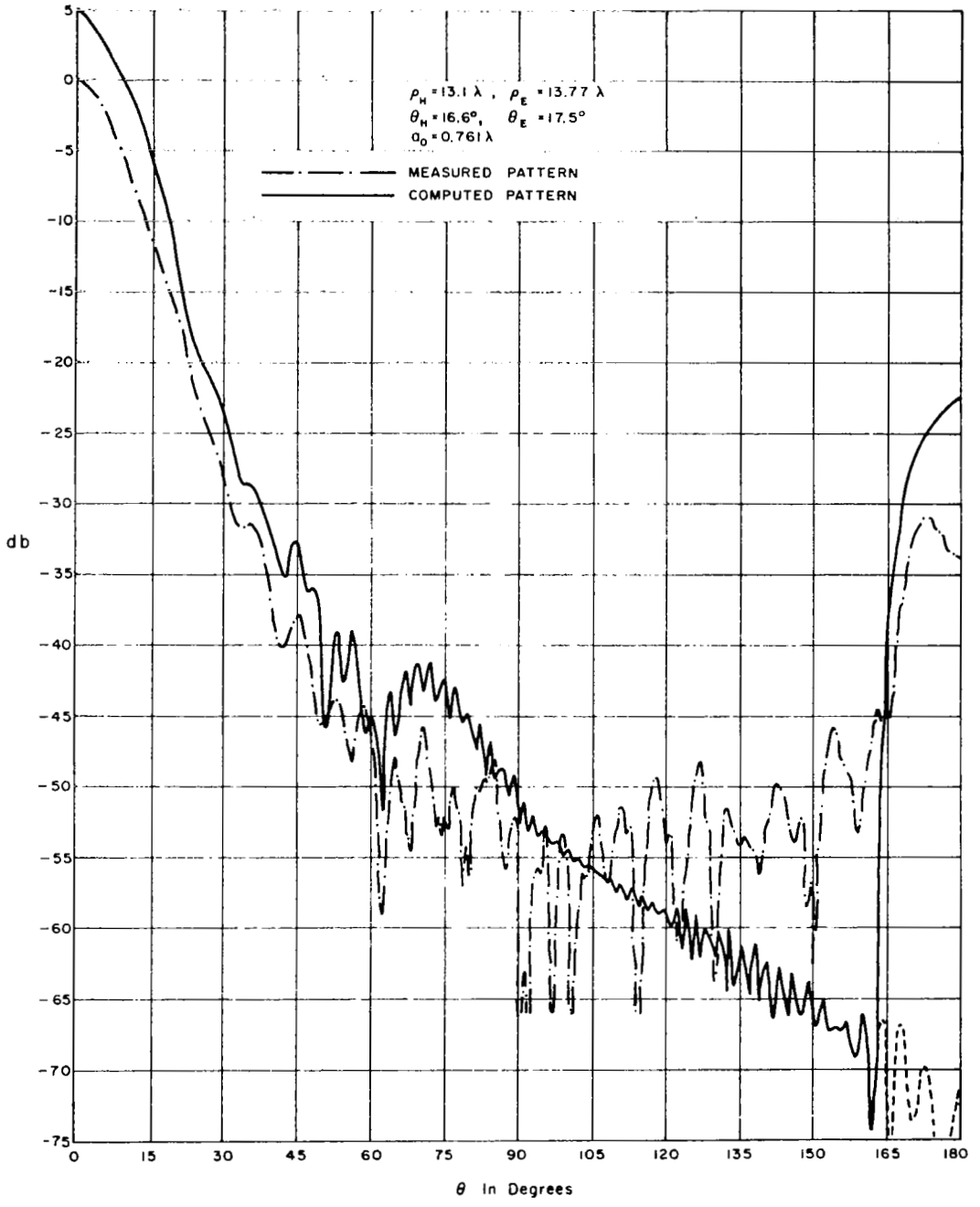

Fig. 19. H-plane patterns of horn.

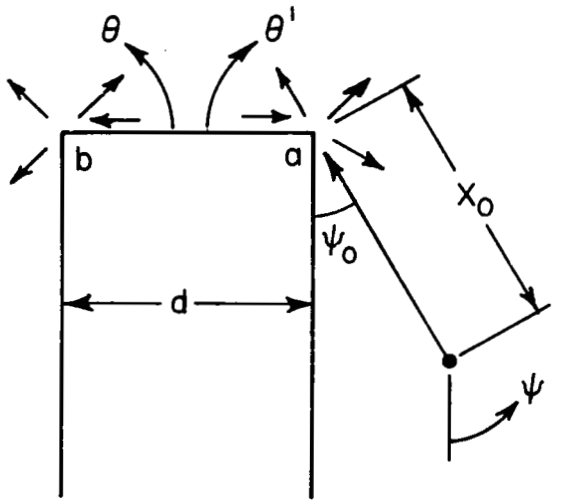

Fig. 20. Diffraction by rectangular edge.

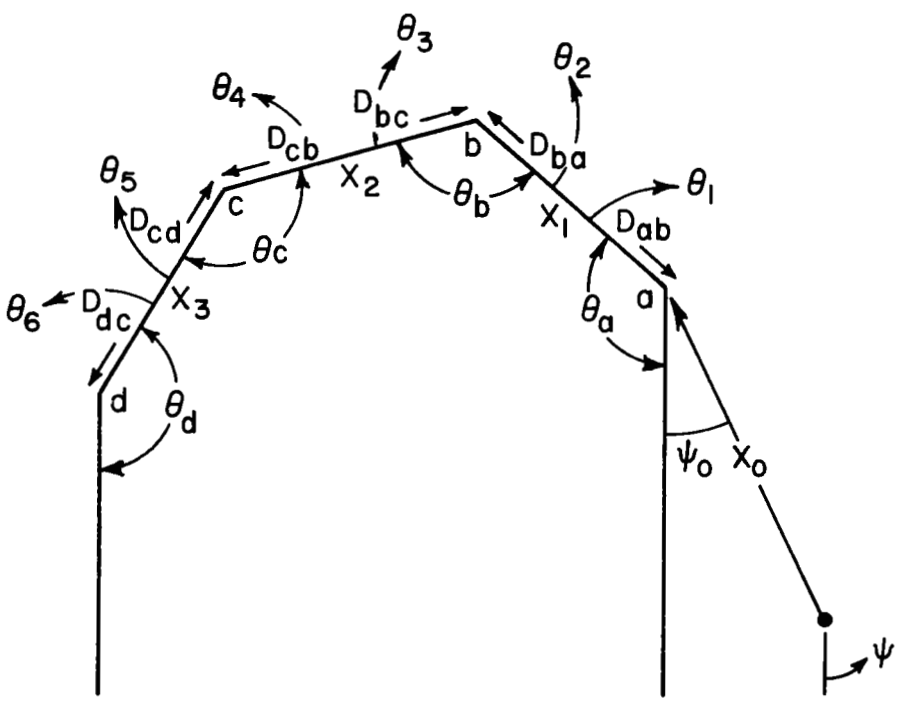

Fig. 21. Polygonal edge.

The unknown illuminating rays are shown in Fig. 21. Hence the diffracted waves from each corner may be expressed as

$$(58) \qquad D_a(\psi) = v_B(x_o, \psi - \psi_o) + v_B(x_o, \psi + \psi_o) + D_{ab}\, v_B(x_1, \theta_1)$$

$$D_b(\psi) = D_{ba}\, v_B(x_1, \theta_2) + D_{bc}\, v_B(x_2, \theta_3)$$

$$D_c(\psi) = D_{cb}\, v_B(x_2, \theta_4) + D_{cd}\, v_B(x_3, \theta_5)$$

$$D_d(\psi) = D_{dc}\, v_B(x_3, \theta_6) \,.$$

Six simultaneous linear equations can be formulated in terms of the six illuminating rays as follows:

$$(59) \qquad D_{ab} = D_b(\pi - \theta_a) = D_{ba}\, v_B(x_1, 0) + D_{bc}\, v_B(x_2, 2\pi - \theta_b)$$

$$D_{ba} = D_a(2\pi - \theta_a) = v_B(x_o, 2\pi - \theta_a - \psi_o)$$

$$+ v_B(x_o, 2\pi - \theta_a + \psi_o) + D_{ab}\, v_B(x_1, 0)$$

$$D_{bc} = D_c(\theta_c + \theta_d - \pi) = D_{cb}\, v_B(x_2, 0) + D_{cd}\, v_B(x_3, 2\pi - \theta_c)$$

$$D_{cb} = D_b(3\pi - \theta_a - \theta_b) = D_{ba}\, v_B(x_1, 2\pi - \theta_b) + D_{bc}\, v_B(x_2, 0)$$

$$D_{cd} = D_d(\theta_d) = D_{dc}\, v_B(x_3, 0)$$

$$D_{dc} = D_c(\pi + \theta_d) = D_{cb}\, v_B(x_2, 2\pi - \theta_c) + D_{cd}\, v_B(x_3, 0) \,.$$

After the illuminating rays are solved from Eq.(59) the diffracted wave from each corner may be obtained from Eq. (58). By inclusion of the appropriate phase factors to refer each diffracted wave to the same point superposition may be used to obtain the total diffraction pattern. The diffraction patterns for three thick wall configurations are given in Fig. 22.

It is evident that the thick wall of Fig. 21 is a special form of a polygonal cylinder. In fact this appears to be a practical method for computing diffraction by polygonal cylinders for perpendicular polarization and hence radar cross sections of such bodies. A limitation to treating polygonal cylinders by superposition of diffractions from each of the

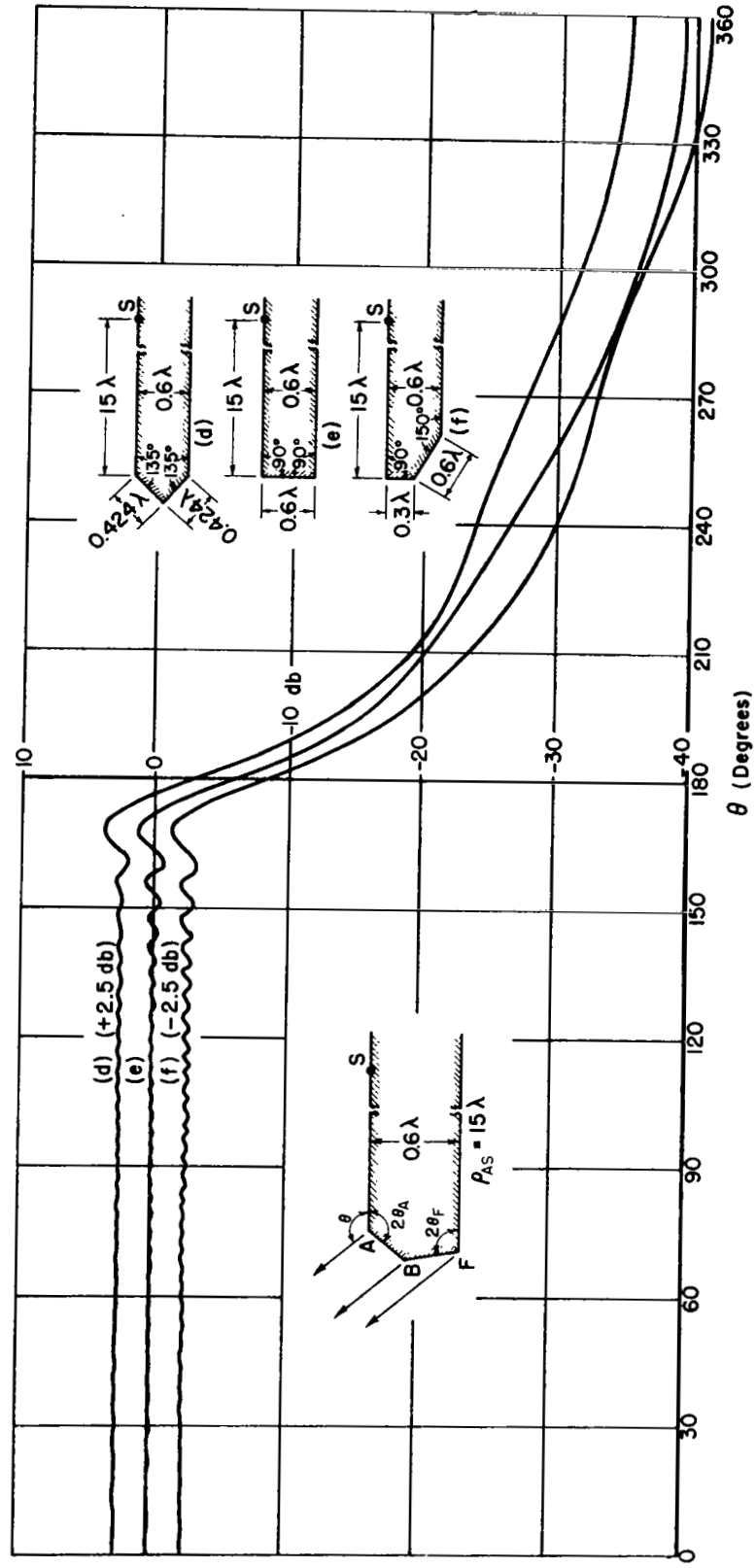

Fig. 22. Diffraction patterns for thick walls.

corners is that the assumption of localized edge effects may be violated for small dimensions between corners - particularly for large wedge angles. Thus the diffraction by a corner cannot be treated the same as a line source at the corner if the adjacent corner from which a subsequent diffraction is to be determined is very close - about a quarter of a wavelength for sharp corners and longer dimensions for shallow corners.

D. Radiation Patterns of Rectangular Waveguides

The principal-plane radiation patterns of a rectangular waveguide truncated perpendicular to its axis have been analysed using the techniques described[17]. The diffraction from the rectangular waveguide is analysed by representing the dominant waveguide mode (TE_{01}) as a combination of plane waves and computing the diffraction from the pairs of edges as two parallel-plate waveguides. The two parallel-plate waveguides are superimposed to form a rectangular waveguide and the interactions which arise from the combination are considered.

In the treatment of diffraction by the edges of a rectangular waveguide, incidence which is not normal to the edge must be considered. Keller[1, 2] has treated this problem by extending Fermat's principle to edge diffraction in three dimensions through the following assumption: "A singly diffracted ray connecting two points is a curve whose length is stationary among all curves connecting these two points and having one point on the edge." As a consequence of this extended principle, a ray normally incident upon the edge of a wedge generates a family of diffracted rays which lie in a disk having the edge as its axis. Also a ray incident obliquely at an angle γ to the edge generates diffracted rays which lie on a cone with the edge as its axis and the half-angle of the cone equal to the angle between the incident ray and the edge. These two cases are shown in Fig. 23. For diffraction in three dimensions the two-dimensional diffraction coefficients must be multiplied by the factor $1/\sin\gamma$ to take into account the distribution of energy around the cone of diffracted rays[1, 2].

The diffraction techniques which have been applied are of a two-dimensional nature and thus do not give the diffraction which occurs in the third dimension for edges of finite length. This technique yields diffracted rays which are parallel, having been derived for an infinite wedge. However, it will be assumed that the diffraction in the dimension in which the rays are parallel is the same as the radiation pattern of a line source of finite length. This assumption takes into account the distribution of energy in three dimensions of each family of parallel diffracted rays due to an edge of finite length.

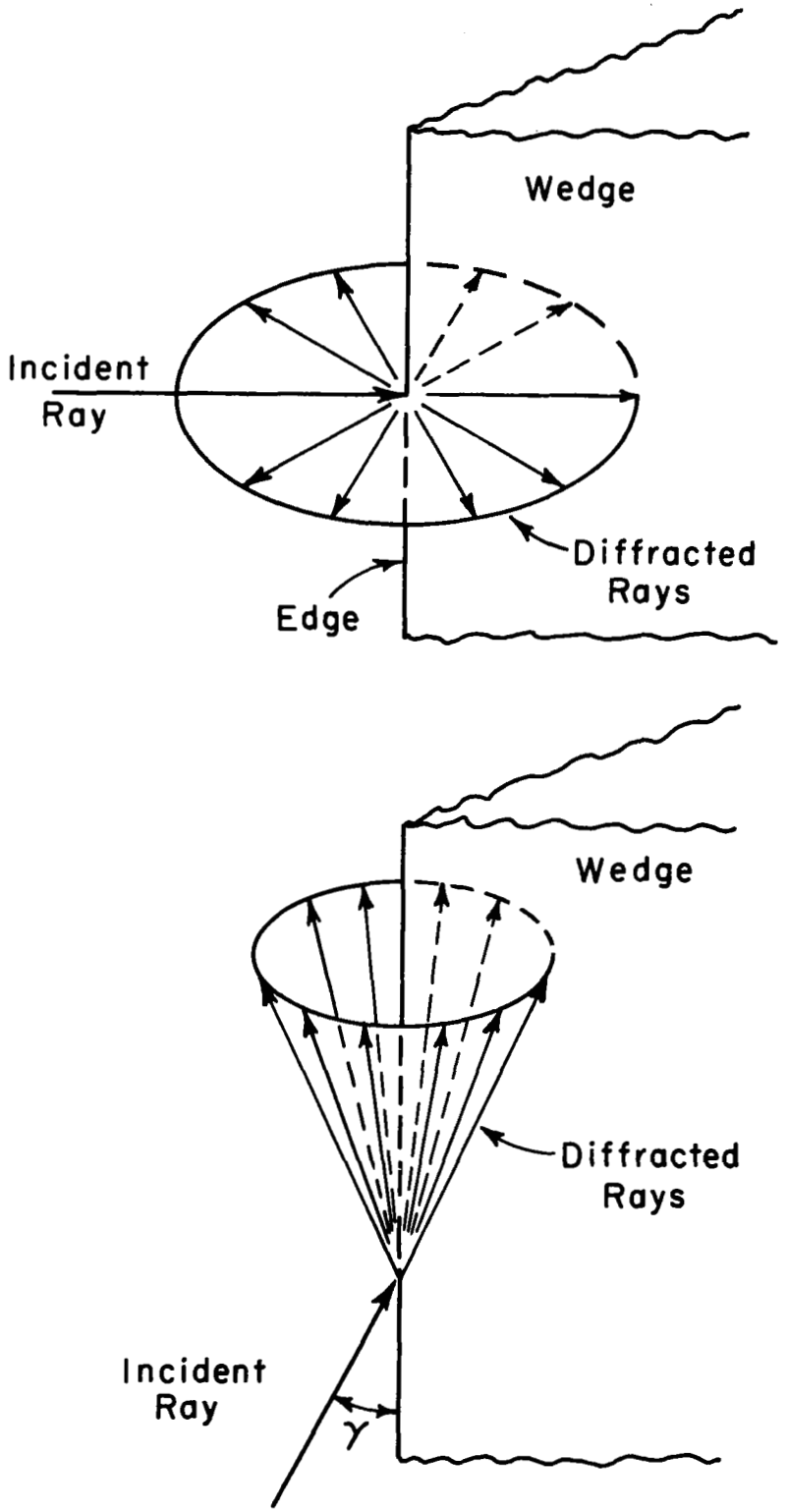

Fig. 23. Conical diffraction for oblique incidence.

The far field pattern of an electric current line source of length L, oriented parallel to the z-axis with center at $(x_o, y=0, z_o)$ and having a travelling current of constant magnitude I_o^e with phase constant β is given by[18]

$$(60) \qquad E_\theta(r, \theta, \phi) = j\omega\mu I_o^e L \sin\theta \frac{e^{-jkr}}{4\pi r} e^{j(k\cos\theta - \beta) z_o}$$

$$\cdot e^{jkx_o \sin\theta\cos\phi} \frac{\sin[(k\cos\theta - \beta) L/2]}{[(k\cos\theta - \beta) L/2]}$$

where conventional spherical coordinates are used.

By duality, the far-field of a magnetic current line source may be obtained by the substitutions:

electric		magnetic
$\overline{E}$	$\rightarrow$	$\overline{H}$
μ	$\rightarrow$	ϵ
I_o^e	$\rightarrow$	I_o^m .

The above substitutions do not affect the shape of the field pattern.

The diffraction from each edge of the rectangular waveguide is taken as the pattern multiplication of two factors: the two-dimensional diffraction about the edge times the sin x/x diffraction of a line source of finite length. The polarization properties of the diffraction by the side walls corresponds to those of an electric current line source whereas the top and bottom walls correspond to magnetic line sources. As seen from Eq. (60) the length of each edge weights the relative contribution from the two pairs of edges. The composite diffraction effects are illustrated in Fig. 24. The diffraction about the edges of the side walls is given directly by the parallel-plate diffraction for the TE_{01} mode. The diffraction about the edges of the top and bottom walls is given by TEM guide diffraction but is modified for oblique incidence as shown in Fig. 25. Thus the slant distance S is substituted for h in Eqs. (31) and (39) for the higher order diffracted rays; and the total diffraction by this pair of walls is multiplied by the factor $1/\sin\left(\frac{\pi}{2} - A_o\right)$.

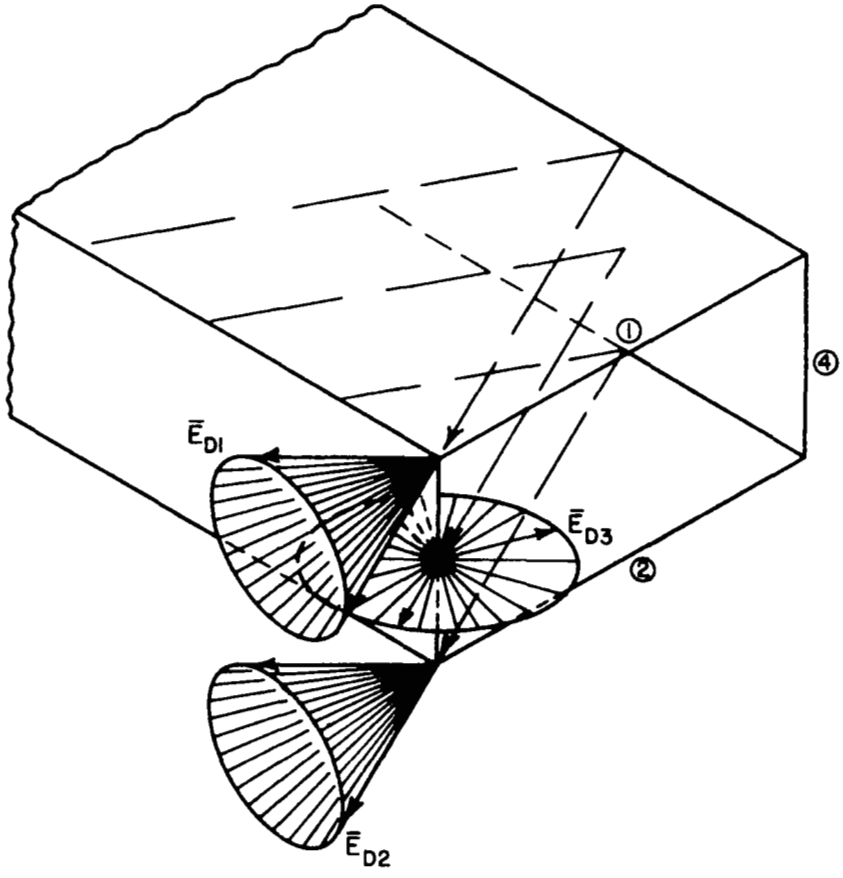

Fig. 24. Diffraction from edges of rectangular waveguide.

The principal-plane patterns calculated by this method were found to be in reasonable agreement with the measured patterns for a conventional X-band waveguide operating at 10 Gc[17]. The E-plane and H-plane patterns are shown in Figs. 26 and 27, respectively.

VI. ANTENNA CONCEPTS APPLIED TO PARALLEL-PLATE WAVEGUIDES

A. Introduction

A major advantage of the diffraction methods described here is that the complete field distribution is available. For example, in the case of the parallel-plate waveguide the field intensities outside the guide can be obtained in terms of the field intensities of the incident wave inside the guide.

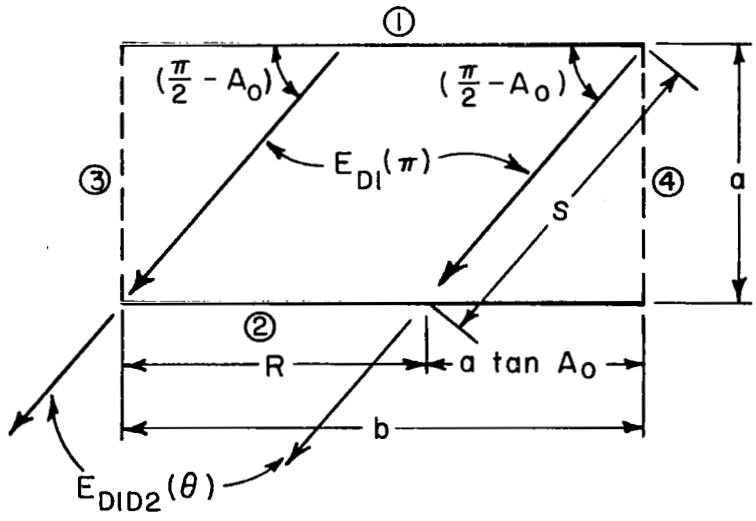

Fig. 25. Interaction between top and bottom edges.

Knowledge of the complete field distribution implies that antenna parameters such as gain, aperture admittance, and coupling between antennas can be explicitly calculated.

In this section various antenna parameters of parallel-plate waveguides are determined in terms of diffraction functions. First, antenna gain is expressed in terms of the diffracted rays from a guide. Next, the near fields of a guide are determined and from this development the coupling between two guides is determined. Finally, the aperture admittance for TEM guides is determined.

B. Antenna Gain and Effective Aperture

Since the scalar functions used here represent the z-component of the field, the magnetic field is appropriate for polarization perpendicular to the edge whereas the electric field is appropriate for parallel polarization. Thus for the TEM mode guide the magnetic field intensity in the far field region can be obtained as

$$H_T = \frac{e^{-j(kr + \pi/4)}}{\sqrt{2\pi kr}} \; R_T = \frac{e^{-jkr}}{\sqrt{r}} \; D_T \tag{61}$$

by including the factor which was previously suppressed. The diffraction coefficient D_T is used in the same context as in the Geometrical Theory of Diffraction.

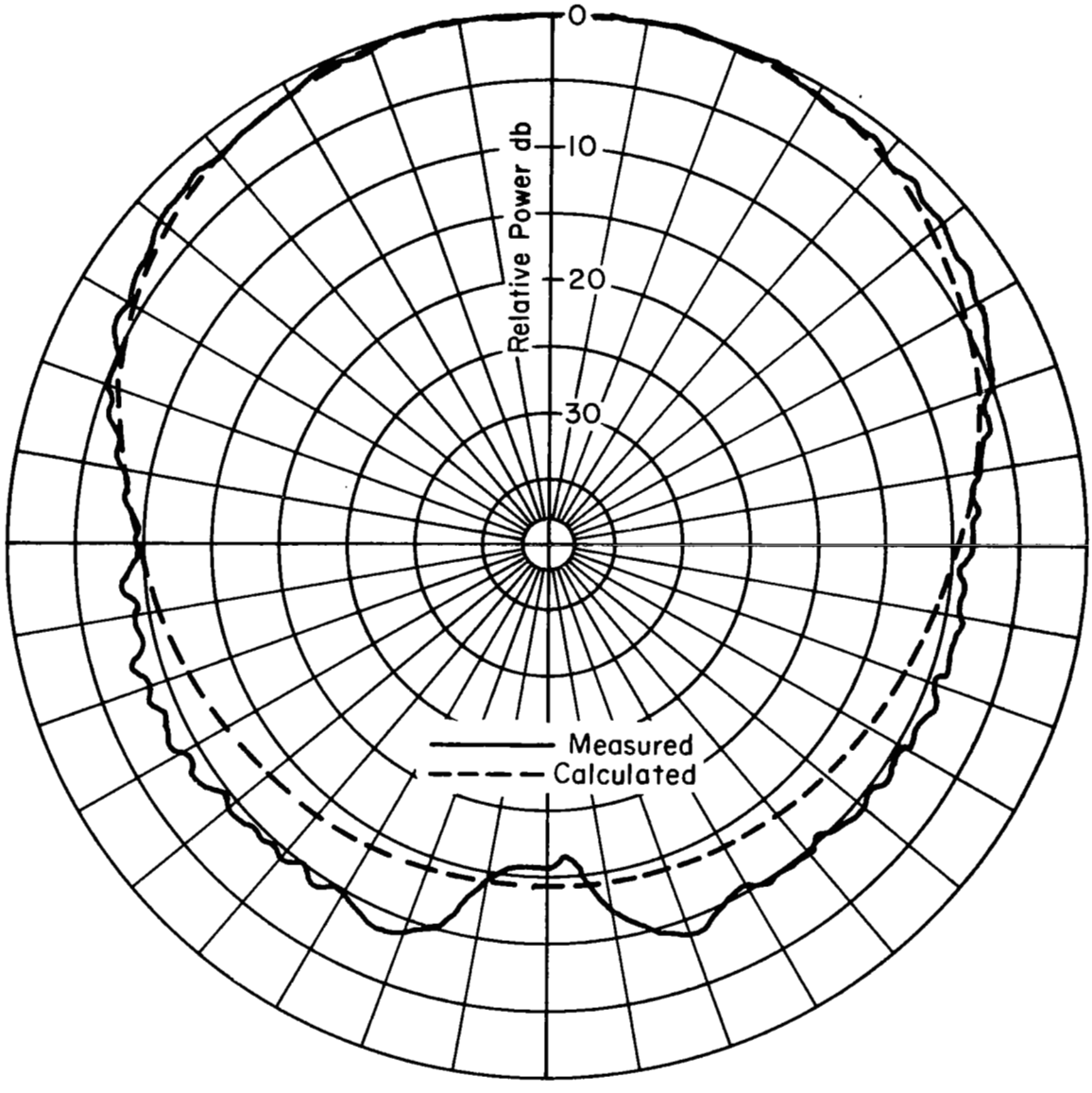

Fig. 26. E-plane pattern of rectangular x-band guide (frequency = 10 Gc.).

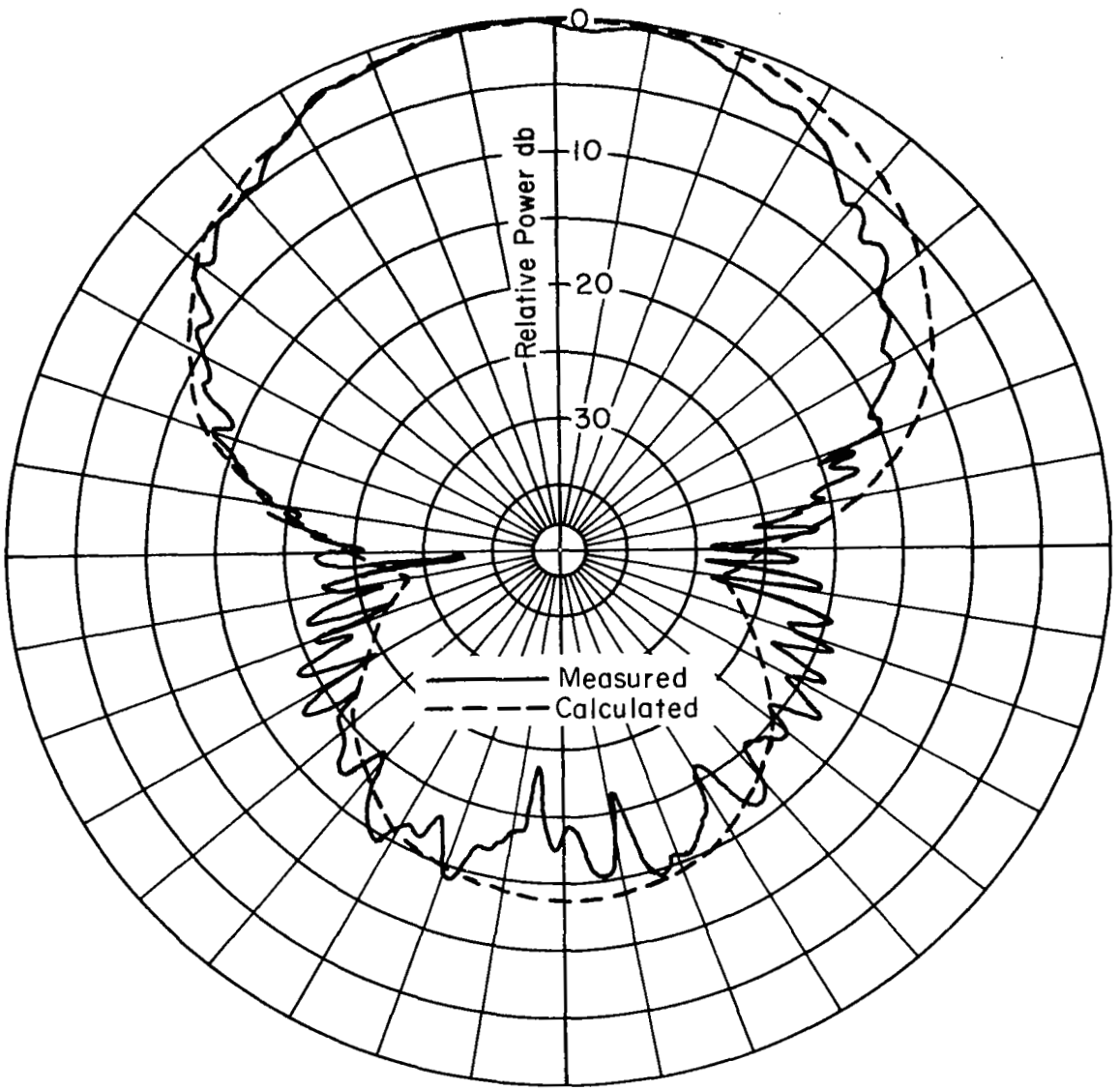

Fig. 27. H-plane pattern of rectangular x-band guide (frequency = 10 Gc.).

The antenna gain of the parallel plate waveguide is calculated from the conventional formula for two-dimensional gain

$$G = \frac{2\pi r S}{P_o} \tag{62}$$

where S is the radiated power density at radius r and P_o is the total power incident in the guide. The power density may be expressed in terms of the diffracted field of Eq. (61) as

$$S = Z_o |H_T|^2 = \frac{Z_o}{r} |D_T|^2 = \frac{Z_o}{2\pi kr} |R_T|^2 \tag{63}$$

where Z_o is the impedance of free space. The power incident in the TEM mode with a unit incident magnetic field is given by

$$P_o = a Z_o \tag{64}$$

where a is the guide width.

Thus the TEM mode antenna gain for a parallel-plate waveguide is given by

$$G = \frac{1}{ka} |R_T|^2 = \frac{2\pi}{a} |D_T|^2 \tag{65}$$

where R_T and D_T are evaluated for the direction in which the gain is determined. The formula for effective aperture width in terms of gain yields

$$W_e = \frac{\lambda}{2\pi} G = \frac{1}{k^2 a} |R_T|^2 = \frac{\lambda}{a} |D_T|^2 \quad . \tag{66}$$

An interesting example to consider is the thin-walled waveguide with normal truncation ($\theta_g = 90°$). The ray on axis ($\theta = 0$) is given by the singly diffracted rays (higher order diffraction is zero on axis) as

(67) $$R_T(0) = \lim_{\theta \to 0} \left(R_{D1}(\theta) + R_{D2}(\theta)\right)$$

$$= \lim_{\theta \to 0} \frac{1}{2} \left[\frac{-1}{\cos \frac{\pi + \theta}{2}} - \frac{e^{jka \cos(\theta + \pi/2)}}{\cos \frac{\pi - \theta}{2}} \right] = jka$$

Consequently, the on-axis gain is

(68) $$G(0) = ka$$

The corresponding effective aperture width for $\theta = 0$ is the guide width a. This is readily verified by considering the guide with a plane wave incident from $\theta = 0$; the guide simply receives the portion of the plane wave which propagates between the waveguide walls.

The preceding equations of this section are applicable to the TE_{01} mode if the values appropriate for the TE_{01} mode rays are used and the magnetic field H_T is replaced by the electric field E_T. For a unit-amplitude electric field intensity in each plane wave component of the TE_{01} mode the distribution across the guide of the incident electric field is $2 \cos A_o \cos \frac{2\pi x}{a}$. Thus the power incident in the TE_{01} mode is obtained by integration as

(69) $$P_o = 2a\, Y_o \cos A_o$$

where A_o is the reflection angle of the TE_{01} plane waves and Y_o is the admittance of free space. Thus the formulas for antenna gain and effective aperture width for the TE_{01} mode become

(70) $$G = \frac{|R_T|^2}{2ka \cos A_o} = \frac{\pi |D_T|^2}{a \cos A_o}$$

and

(71) $$W_e = \frac{|R_T|^2}{2k^2 a \cos A_o} = \frac{\lambda |D_T|^2}{2a \cos A_o} .$$

C. Near Fields

In the treatment of coupling between antennas the field intensities in the near field region are of interest. The singly diffracted rays discussed in Section IV are valid only for the far field region. However, expressions for the singly diffracted rays which are valid in the near field region can be obtained by using the diffraction form V_B. For example, the fields resulting from the singly diffracted rays are given by

$$H_{D1}(r_1, \theta_1) = V_B(r_1, \pi + \theta_1) \tag{72}$$

and

$$H_{D2}(r_2, \theta_2) = e^{-jka \cot \theta_g} V_B(r_2, \pi - \theta_2) \tag{73}$$

where r_1, θ_1 and r_2, θ_2 are measured from edges 1 and 2, respectively.

The fields due to higher order diffracted rays may be obtained by using the form of cylindrical wave diffraction given in Eq. (22). Thus the expressions for the total higher order diffracted fields which are valid in near field regions are given by

$$H_{HD2}(r_2, \theta_2) = \frac{e^{-j\pi/4}}{\sqrt{2\pi k}} R_{1G} \frac{e^{-jk(r_2 + h)}}{\sqrt{r_2 + h}} e^{jk \frac{r_2 h}{r_2 + h}} \cdot \left[V_B\left(\frac{r_2 h}{r_2 + h}, \pi - \theta_2 - \theta_g\right) + V_B\left(\frac{r_2 h}{r_2 + h}, \pi - \theta_2 + \theta_g\right) \right] \tag{74}$$

and

$$H_{HD1}(r_1, \theta_1) = \frac{e^{-j\pi/4}}{\sqrt{2\pi k}} R_{2G} \frac{e^{-jk(r_1 + h)}}{\sqrt{r_1 + h}} e^{jk \frac{r_1 h}{r_1 + h}} \cdot \left[V_B\left(\frac{r_1 h}{r_1 + h}, \theta_1 + \theta_g\right) + V_B\left(\frac{r_1 h}{r_1 + h}, 2\pi + \theta_1 - \theta_g\right) \right] \tag{75}$$

(Eq. (75) continues on next page)

$$+\frac{e^{-j\pi/4}}{\sqrt{2\pi k}}\, R_{1P}\, \frac{e^{-jk(r_1+2a)}}{\sqrt{r_1+2a}}\quad e^{\,jk\,\frac{2ar_1}{r_1+2a}}$$

$$\cdot\left[V_B\left(\frac{2ar_1}{r_1+2a},\ \frac{\pi}{2}+\theta_1\right)+V_B\left(\frac{2ar_1}{r_1+2a},\ \frac{3\pi}{2}+\theta_1\right)\right]$$

where R_{1G}, R_{2G} and R_{1P} are the illuminating rays given in Eq. (41).

The total diffracted wave from each edge is thus given as

(76) $$H_1(r_1,\ \theta_1) = H_{D1}(r_1,\ \theta_1) + H_{HD1}(r_1,\ \theta_1)$$

and

(77) $$H_2(r_2,\ \theta_2) = H_{D2}(r_2,\ \theta_2) + H_{HD2}(r_2,\ \theta_2)\,.$$

The field at point P is given by superposition of the components from each edge and the reflections, as

(78) $$H_T(P) = H_1(r_1,\ \theta_1) + H_2(r_2,\ \theta_2) + H_1(r_f,\ \theta_f)$$

where r_f, θ_f are the coordinates of the image of point P in the lower wall. The same regions still apply for each term as given in Eq. (43). The phase factors of Eq. (42) do not appear because they are taken into account by use of the near field forms of the diffraction.

D. Coupling between Guides

In the treatment of antenna admittance and coupling between antennas power transfer is significant. Power transfer may be expressed in terms of modal currents or voltages; this permits expression of phase as well as magnitude of the power transfer. The phase of the modal current in the TEM waveguide is defined as the phase of the wave at one of the aperture edges. The consideration of phase is necessary to provide information on standing wave null positions for admittance calculations; and to allow

superposition of mutual coupling between multiple antenna elements in order to calculate the total coupling.

Since the transmission line impedance of the TEM guide is the same as that of free space, Z_o, the modal current of the incident wave is obtained from Eq. (64) as

$$I_o = \sqrt{a} \quad . \tag{79}$$

The modal current induced in the guide by an incident plane wave of electric field intensity Hi is obtained from Eq. (66) as

$$I_e = \sqrt{\frac{\lambda}{a}}\, D_T\, Hi\; e^{-j\pi/4} \quad . \tag{80}$$

As an example of calculation of mutual coupling the formulation of coupling between two parallel plate waveguides is given below. Consider the coupling between the two guides shown in Fig. 28. The diffraction which occurs at each of the apertures is discussed previously; each aperture edge is an apparent line source. In the formulation of coupling the transmitting guide is replaced by equivalent line sources. Each equivalent source has an omnidirectional pattern and the radiated field is the same as that which is radiated in the direction of the receiving

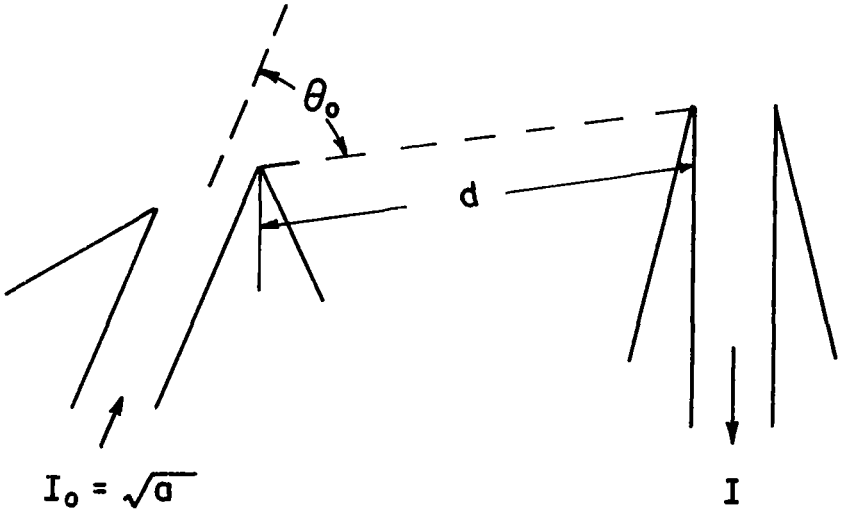

Fig. 28. Coupling between parallel-plate waveguides.

guide by the edge it replaces. The modal current induced in the receiving guide by a line source completes the information needed for coupling.

The simplified case in which the outside edge of the transmitting aperture is outside the line-of-sight between the inside edges will be considered here. Thus the transmitting guide may be replaced by a single line source which radiates a field given by

$$I_1 \frac{e^{-jkr + j\pi/4}}{\sqrt{2\pi r}} = H_{T0}(\theta_o) \tag{81}$$

as shown in Fig. 29. The modal current I_1 is that of the equivalent line source with an antenna impedance Z_o and may be expressed in the terminology of Eq. (61) as

$$I_1 = \frac{e^{-j\pi/2}}{\sqrt{k}} R_{T0}(\theta_o) = \sqrt{2\pi}\, D_{T0}(\theta_o)\, e^{-j\pi/4} \tag{82}$$

where R_{T0} is the total diffracted ray from the transmitting guide in the direction of the receiving guide.

The modal current induced in the receiving guide by the equivalent line source is obtained by application of reciprocity. The modal current induced in the line source by the receiving guide excited by the modal current I_1 is first determined. The power received by a line source at point Q as shown in Fig. 30(a) is given by

$$P = \frac{\lambda}{2\pi} |H_{T1}|^2 Z_o \tag{83}$$

where $\lambda/2\pi$ is the effective aperture of the line source and H_{T1} is the field at point Q due to the modal current I_1 in the guide. The field H_{T1} is given by

$$H_{T1} = \frac{I_1}{\sqrt{a}} H_T(Q) \tag{84}$$

where $H_T(Q)$ is the total field at point Q for a wave incident in the guide which has a unit-amplitude magnetic field and thus a modal current of $\sqrt{a}$.

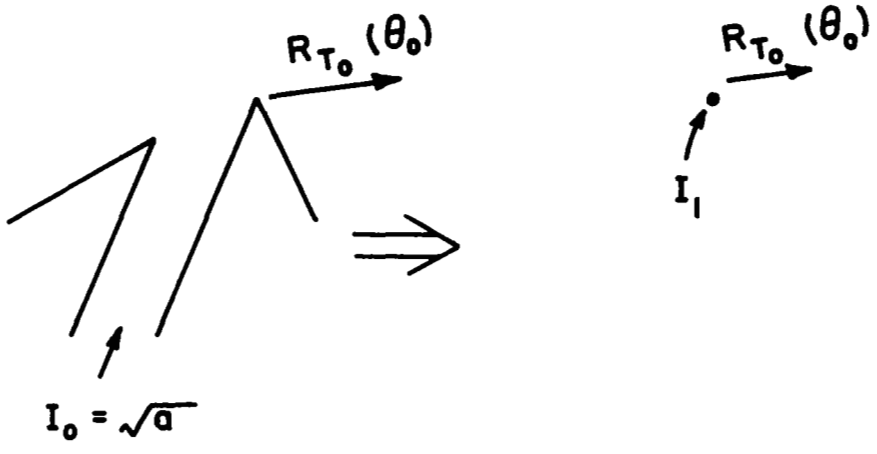

Fig. 29. Equivalent line source for transmitting guide.

If point Q is in the far field region of the guide aperture the field is given by Eqs. (61) and (42). For points in the near field the formulation for $H_T(Q)$ is given by Eq. (78).

The modal current received by the line source is thus given by

$$I = \sqrt{\frac{\lambda}{2\pi}}\, H_{T1} = \sqrt{\frac{\lambda}{2\pi a}}\, I_1\, H_T(Q) \quad . \tag{85}$$

By reciprocity the same current I is induced in the receiving guide by the line source with excitation I_1 as shown in Fig. 30(b).

The coupling between the guides is obtained from Eqs. (82) and (85) as

$$\frac{I}{I_0} = \frac{\sqrt{\lambda}}{a}\, D_{T0}(\theta_0)\, H_T(Q)\, e^{-j\,\pi/4} \quad . \tag{86}$$

In brief, Eq. (86) gives the TEM mode coupling between the two parallel-plate guides shown in Fig. 28 where $D_{T0}(\theta_0)$ is the diffraction coefficient of the transmitting guide as given by Eqs. (42) and (61) and $H_T(Q)$ is the field of the receiving guide at point Q as given in Eq. (78).

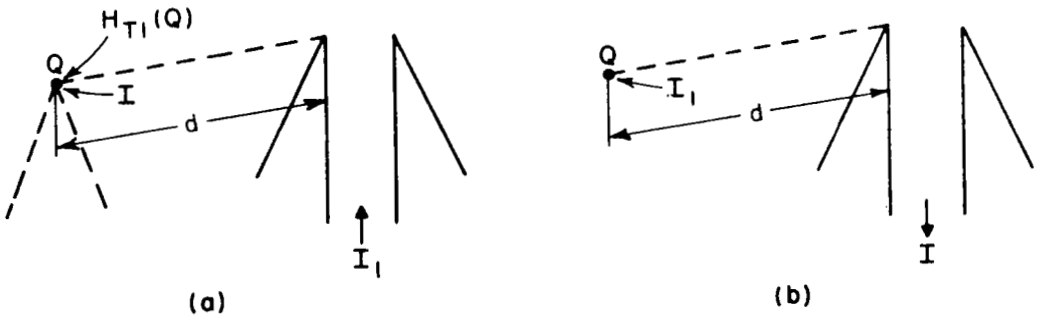

Fig. 30. Use of reciprocity to obtain response of guide to line source.

Equation (86) is valid provided the wedge angles are not too large. However, the case for which the wedge surfaces coincide to form a ground plane between the guides can be derived in a similar manner. The coupling derivation for the ground plane case gives 1/2 that of Eq. (86) (6 db lower).

The coupling for the TE_{o_1} mode is obtained in the same manner and is given by

$$\frac{I}{I_o} = \frac{\sqrt{\lambda}}{2a\cos A_o} \; D_{T0}\;(\theta_o)\; E_T\;(Q)\; e^{-j\pi/4} \quad . \tag{87}$$

The diffraction coefficient $D_{T0}\,(\theta_o)$ is obtained by using Eqs. (49) through (53) in Eq. (42). The field $E_T(Q)$ at point Q from the receiving guide is expressed in the same manner as H_T in Eq. (78).

Sample calculations of coupling are shown in Figs. 31 and 32. In Fig. 31 the TEM mode coupling between two normally truncated guides ($\theta_g = 90°$, guide width = $0.338\,\lambda$) oriented parallel as shown is given as a function of spacing between the guides. The curve of measured coupling was obtained by use of wide-angle sectoral horns[19]. Similarly, the TE_{01} coupling between two guides (guide width = $0.761\,\lambda$) mounted without ground plane is given in Fig. 32.

E. Aperture Admittance

The TEM mode aperture admittance of the thin-walled parallel-plate guide can be formulated by identifying the two situations shown in Fig. 33.

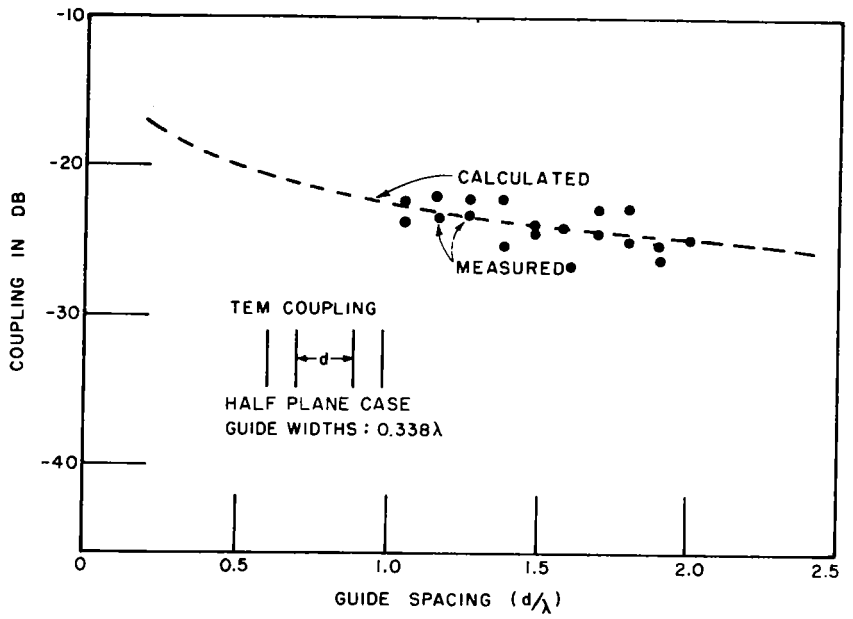

Fig. 31. TEM mode coupling.

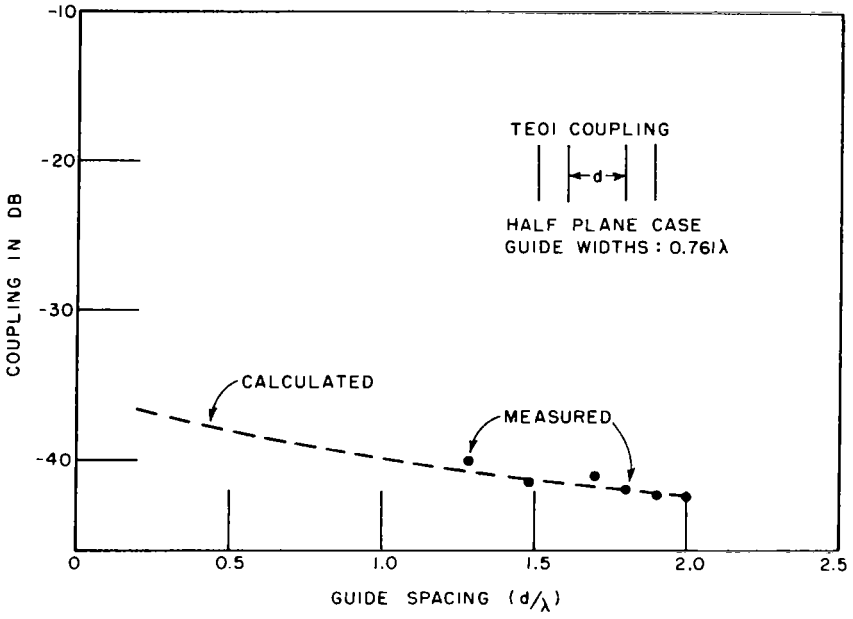

Fig. 32. TE_{01} mode coupling.

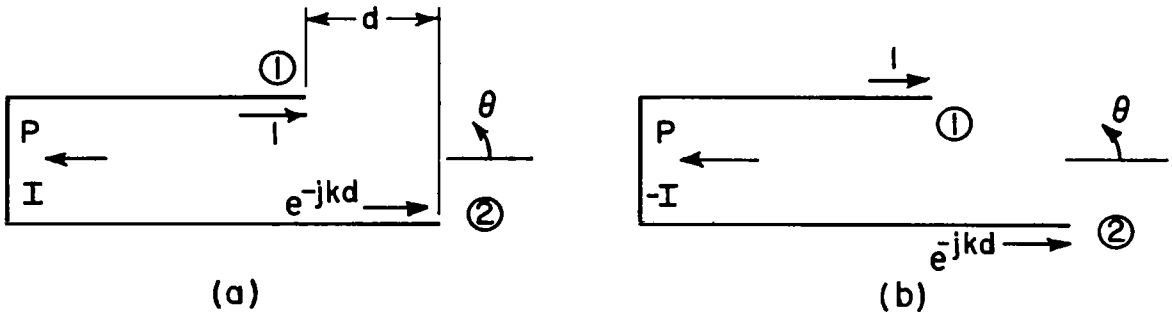

Fig. 33. Plane wave incidence from inside and outside the guide.

Because of the symmetry of half-plane diffraction, the diffracted field distributions of (a) and (b) are identical except for sign. Thus the power reflected back into the guide by mismatch (Fig. 33(a)) is the same as that received by the guide for a plane wave incident outside the guide from the 180° direction.

The power P received by the guide in Fig. 33(b) can be determined from the effective aperture width. The diffraction coefficients from edges 1 and 2 are given by

(88) $$D_1 = \frac{e^{-j\pi/4}}{\sqrt{2\pi k}} R_1(180°)$$

and

(89) $$D_2 = \frac{e^{-j\frac{\pi}{4}}}{\sqrt{2\pi k}} R_2(-180°)$$

where R_1 and R_2 are obtained from Eqs. (32) and (40). With this guide the diffracted rays from edges 1 and 2 are again diffracted from the 90° corners of the guide as shown in Fig. 34; thus the total diffraction coefficient in the 180° direction is given by

(90) $$D_T = \tfrac{1}{2}\left(D_1 + e^{-jkd} D_2\right)$$

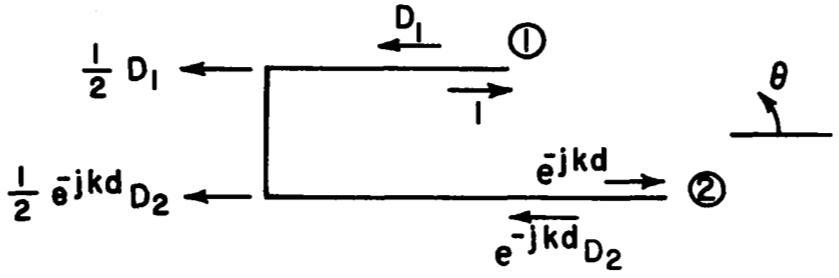

Fig. 34. Diffraction in the 180° direction.

where e^{-jkd} is the phase factor resulting from choice of edge 1 as phase reference. The length of the guide is chosen to be much greater than the guide width so that multiple diffractions between the waveguide corners are negligible compared to the single diffractions.

Thus the induced modal current corresponding to the reflected power caused by aperture mismatch is obtained from Eq. (80) as

$$I = -\tfrac{1}{2}\sqrt{\frac{\lambda}{a}}\left[D_1(\phi = 2\pi) + e^{-jkd}\, D_2(\phi = 2\pi)\right] e^{-j\pi/4} \tag{91}$$

where the minus sign results from the difference in the two situations of Fig. 33 (a) and (b) and ϕ is used in the same convention as in $v_B(r, \phi)$. The induced modal current may be written in a form which yields a better physical interpretation:

$$I = \tfrac{1}{2}\sqrt{\frac{\lambda}{2\pi ka}}\left[R_1(-180°) + e^{-jkd}\, R_2(180°)\right] e^{-j\pi/2} \tag{92}$$

$$= \tfrac{1}{2}\sqrt{\frac{\lambda}{a}}\left[D_1(\phi = 0) + e^{-jkd}\, D_2(\phi = 0)\right] e^{-j\pi/4} \quad .$$

In Eq. (92) the induced modal current is obtained in terms of the rays diffracted back along the inside instead of the outside of the waveguide walls.

The reflection coefficient of the aperture with phase referred to edge is thus given by

(93) $$\Gamma = \frac{I}{I_o} = \frac{1}{2} \frac{\sqrt{\lambda}}{a} \left[D_1(\phi = 0) + e^{-jkd} D_2(\phi = 0) \right] e^{-j\pi/4}$$

where $D_1(\phi = 0)$ and $D_2(\phi = 0)$ are the total diffraction coefficients for edges 1 and 2 corresponding to the rays diffracted back along the inside of the waveguide walls. The normalized aperture admittance of the TEM guide can be determined from the reflection coefficient by the transmission line formula as

(94) $$Y_A/Y_o = \frac{1 - \Gamma}{1 + \Gamma} \quad .$$

The magnitude of the TEM reflection coefficient as calculated by Eq. (93) is given in Fig. 35 for the thin-walled guide as a function of guide width.

VII. DISCUSSION

The principal feature of this method is the use of geometrical optics techniques to describe diffraction; this approach was introduced in the Geometrical Theory of Diffraction. The characteristics of diffraction by a wedge are such that it can be expressed in terms of the geometrical optics fields and a cylindrical wave radiating from the edge of the wedge. The fact that wedge diffraction can be treated as a local edge effect allows structures composed of wedges to be analyzed by superposition.

In the Geometrical Theory of Diffraction, wedge diffraction is normally treated in terms of asymptotic plane wave coefficients. The principal modification of the Geometrical Theory of Diffraction was the extension of the method to include diffraction for cylindrical wave incidence. It is this extension which allows structures of practical dimensions to be treated. For example, multiple diffractions can be described more accurately, particularly in regions near shadow boundaries.

A major problem in treating diffraction of a cylindrical wave by a wedge is the determination of formulations of the solution which are practical for computational purposes. In this regard the formulation of Pauli is useful in most cases; however, the higher order terms are not always negligible. For cases in which Pauli's formulation is not practical to use the formulation in terms of cylindrical wave functions successfully fills the deficiency.

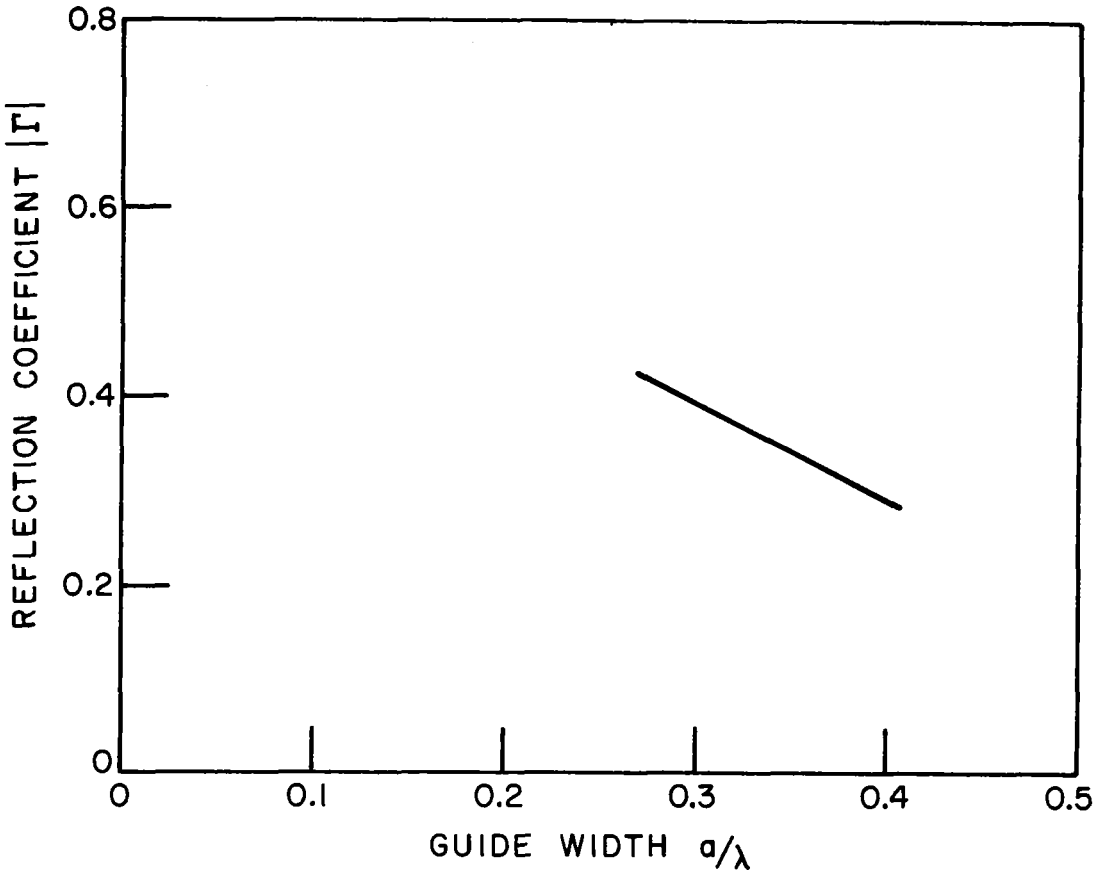

Fig. 35. Reflection coefficient of thin-walled guide.

Another significant development is the concept in which the total effects of higher order diffractions may be summed. This concept simplifies formulation of solutions and provides for more practical computation of problems in which interactions are large.

The nature of this method allows more practical and accurate treatment of many problems than is available by conventional techniques. A common approach to electromagnetic problems is to use the fact that, by equivalence principles, the fields in the region of interest may be expressed in terms of the total fields on some surface. The usual approximation involved is to assume the total fields on the surface to be given by the physical optics fields. For example, the fields in the aperture of a reflector antenna are usually obtained by the reflection of the feed pattern and the resultant fields are integrated to obtain the radiation pattern. Similarly, the aperture fields of a horn antenna are usually approximated

by modes which propagate between the horn walls. In either case the effects at the aperture edges cannot be practically treated; and thus fields in the hemisphere to the rear of the aperture (backlobe regions) cannot be determined. The conventional method of aperture integration generally yields good results in the region near the main beam for most antennas. However, the physical optics approximation to the aperture fields of a small antenna may not be satisfactory. For example, small waveguide apertures cannot be accurately treated by conventional techniques; but the edge diffraction method accurately describes the edge effects and the interactions between the edges.

Another major advantage of this method is that the fields may be directly related to the incident fields. This feature allows analytical determination of antenna parameters such as gain, aperture admittance and coupling between antennas in specific terms. By comparison, the treatment of near field coupling between antennas by conventional techniques is generally a very difficult problem. In scattering problems this feature provides the scattered fields in terms of the incident fields and thus scattering apertures and radar cross sections may be analytically determined.

By these diffraction techniques fields can be determined in regions within an antenna as well as in far field and near field regions. For example, the fields propagating between the walls of a horn can be determined. Similarly, the scattered fields inside a truncated waveguide may be determined. But it is impractical to treat regions in the guide which are at significant distances from the aperture because of the numerous reflections between the guide walls. However, the response of a guide to an external source may be determined for a specific waveguide mode by use of the principle of reciprocity. In fact, reciprocity is an important tool in diffraction techniques. It is useful in relating situations so that desired information can be determined. For example, the diffraction by a cylindrical wave can be related to plane wave diffraction. Also the determination of response of a guide by use of reciprocity allows mutual coupling and aperture admittance to be treated.

The area of curved surfaces is not treated in this publication. Much research has been accomplished in the application of geometrical techniques of diffraction by curved surfaces[1, 2, 20, 21, 22]. However, the treatment of doubly curved surfaces is more complicated and has not reached the state of refinement that wedge diffraction has.

There are still many limitations and unexplored areas regarding these diffraction techniques. They are primarily useful for two-dimensional situations although they may be applied to some three-dimensional problems, e. g., the pyramidal horn and the rectangular waveguide.

The various limitations suggest possible future extensions of diffraction techniques. For example, further refinements for treating curved surfaces and dielectric materials are needed. A valuable tool for treating dielectric materials would be a practical formulation for diffraction by a dielectric wedge with one surface coated by a metallic sheet. This tool would allow dielectric-filled waveguides to be analyzed. Also the treatment of rectangular waveguides by corner diffraction techniques would appear to be more desirable than the treatment described here.

Another major area of extension is the diffractions resulting from illuminations other than uniform cylindrical or plane wave incidences. It appears possible to treat non-uniform illumination in two dimensions by multipole sources. The three-dimensional problem of diffraction by a circular waveguide aperture requires treatment of the illumination resulting from various waveguide modes as well as the effects of the curved edges.

The diffraction techniques discussed in this publication provide a new approach to electromagnetic theory, with many advantages over conventional techniques. These techniques need to be extended into many new areas of application. Although it is easy to determine the needs it may be difficult to fulfill many of them.

ACKNOWLEDGEMENTS

The author gratefully acknowledges the contributions and research of R. B. Dybdal, P. M. Russo, C. E. Ryan, Jr., L. Tsai and J. S. Yu, who participated in the various research developments which are summarized here. The helpful comments of Dr. L. Peters, Jr., who reviewed this manuscript and the encouragement of Dr. C. A. Levis who foresaw the need for this publication are sincerely appreciated.

REFERENCES

1. Keller, J. B., "Geometrical Theory of Diffraction", J. Opt. Soc. Am., 52, No. 2, February, 1962, pp. 116-130.

2. Keller, J. B., "Diffraction by an Aperture", J. Appl. Phys., 28, No. 4, April, 1957, pp. 426-444.

3. Pauli, W., "On Asymptotic Series for Functions in the Theory of Diffraction of Light", Phys. Rev., 54, 1 December 1938, pp. 924-931.

4. Obha, Y., "On the Radiation Patterns of a Corner Reflector Finite in Width", IRE Trans. on Antennas and Propagation, AP-11, No. 2, March 1963, pp. 127-132.

5. Sommerfeld, A., Optics, Academic Press, Inc., New York, 1954, pp. 245-265.

6. Oberhettinger, F., "On Asymptotic Series for Functions Occurring in the Theory of Diffraction of Waves by Wedges", J. Math. and Phys. 34, 1955, pp. 245-255.

7. Harrington, R. F., Time-Harmonic Electromagnetic Fields, McGraw-Hill Book Co., Inc., New York, 1961, pp. 238-242.

8. Yu, J. S., Rudduck, R. C., "Diffraction by Conducting Walls of Finite Thickness", Report 1767-7, 15 May 1965, Antenna Laboratory, The Ohio State University Research Foundation; prepared under contract AF 30(602)-3269, Rome Air Development Center, Griffiss Air Force Base, New York.

9. Ryan, C. E., Jr., Rudduck, R. C., "Calculation of Radiation Pattern of a General Parallel Plate TEM Waveguide Aperture", Report 1394-11, 31 December 1963, Antenna Laboratory, The Ohio State University Research Foundation; prepared under contract AF 33(657)-7829, Aeronautical Systems Division, Wright-Patterson Air Force Base, Ohio, (AD 433 716).

10. Ryan, C. E., Jr., Rudduck, R. C., "Calculation of the Radiation Pattern of a General Parallel-Plate Waveguide Aperture for the TEM and TE_{01} Waveguide Modes", Report 1693-4, 10 September 1964, Antenna Laboratory, The Ohio State University Research Foundation; prepared under contract N62269-2184, U. S. Naval Air Development Center, Johnsville, Pennsylvania.

11. Kraus, J. D., Electromagnetics, McGraw-Hill Book Co., New York, 1953, pp. 445-450.

12. Russo, P. M., Rudduck, R. C., and Peters, L., Jr., "A Method for Computing E-Plane Patterns of Horn Antennas", IEEE Trans. on Antennas and Propagation, AP-13, No. 2, March 1965, pp. 219-224.

13. Yu, J. S., Rudduck, R. C., "The E-Plane Radiation Pattern of an Antenna Model for Horn Antennas", Report 1767-3, 1 April 1965, Antenna Laboratory, The Ohio State University Research Foundation; prepared under Contract AF 30(602)-3269, Rome Air Development Center, Griffiss Air Force Base, New York.

14. Yu, J. S., and Rudduck, R. C., "The H-Plane Radiation Pattern of Horn Antennas", Report 1767-5, 15 May 1965, Antenna Laboratory, The Ohio State University Research Foundation; prepared under Contract AF 30(602)-3269, Rome Air Development Center, Griffiss Air Force Base, New York.

15. Kraus, J. D., Antennas, McGraw-Hill Book Co., Inc., New York, 1950, pp. 375-380.

16. Burke, J. E., and Keller, J. B., "Diffraction by a Thick Screen, A Step and Related Axially Symmetric Objects", EDL-E48, Sylvania Electronic Systems, Contract DA 36-039-SC-78281, March 1960.

17. Ryan, C. E., Jr., Rudduck, R. C., "Calculation of the Far-Field Patterns of a Rectangular Waveguide", Report 1693-7, 20 November 1964, Antenna Laboratory, The Ohio State University Research Foundation; prepared under Contract N62269-2184, U. S. Naval Air Development Center, Johnsville, Pennsylvania.

18. Walter, C. H., Traveling Wave Antennas, McGraw-Hill Book Co., Inc., New York, 1965, p. 32-35.

19. Dybdal, R. B., "Mutual Coupling Between TEM and TE_{01} Parallel-Plate Waveguide Apertures", Report 1693-5, 15 August 1964, Antenna Laboratory, The Ohio State University Research Foundation; prepared under Contract N62269-2184, U. S. Naval Air Development Center, Johnsville, Pennsylvania.

20. Keller, J. B. and Levy, B. R., "Decay Exponents and Diffraction Coefficients for Surface Waves or Surfaces on Non-Constant Curvature", Symposium on Electromagnetic Theory, Professional Group on Antennas and Propagation, Institute of Radio Engineers, December 1959, pp. 552-561.

21. Peters, L., Jr., "Modifications of Geometrical Theory of Diffraction for Non-Cylindrical Curved Surfaces", Report 1815-2, 5 March 1965, Antenna Laboratory, The Ohio State University Research Foundation; prepared under subcontract 28-5041, Lockheed Missiles and Space Company, A Group Division of Lockheed Aircraft Corporation, Sunnyvale, California.

22. Senior, T. B. A. and Goodrich, R. F., "Scattering by a Sphere", Proc. IEE, vol. III, No. 5, May 1964, pp. 907-916.

NASA-Langley, 1966 CR-372